Fall 2020

# Contribution of Submarine Groundwater Discharge to Select Biogeochemical Fluxes in St. Louis Bay, Mississippi

Haley Spaid

# CONTRIBUTION OF SUBMARINE GROUNDWATER DISCHARGE TO SELECT BIOGEOCHEMICAL FLUXES IN ST. LOUIS BAY, MISSISSIPPI

by

Haley Spaid

A Thesis
Submitted to the Graduate School,
the College of Arts and Sciences
and the School of Ocean Science and Engineering
at The University of Southern Mississippi
in Partial Fulfillment of the Requirements
for the Degree of Master of Science

Approved by:

Alan Shiller, Committee Chair
Christopher Hayes
Davin Wallace

December 2020

## ABSTRACT

This thesis assesses the role of submarine groundwater discharge (SGD) in St. Louis Bay, Mississippi. Located along the northern Gulf of Mexico, St. Louis Bay (SLB) is a semi-enclosed bay that is important to the local area for recreation and tourism. SGD is the movement of any water into the water column across the sediment-water interface. In coastal environments, SGD can be a source of a variety of substances including nutrients and pollutants. In this study, a steady state mass balance approach was used to quantify SGD flux for SLB using $^{223}Ra$, $^{224}Ra$, and Ba. Using the water volume flux data calculated from the mass balances and groundwater endmembers for $CH_4$, $NO_3$, $NO_2$, $NH_4$, $PO_4$, and $SiO_3$, fluxes from SGD of these select substances were calculated. It was found that the average water volume flux of SGD was $5.3 \cdot 10^5$ $m^3$ $d^{-1}$ and delivers approximately 1300 mol $d^{-1}$ during the sampling period. SGD was also found to be a significant source of $NO_3$ (17-60 kmol $d^{-1}$) and $PO_4$ (12-42 kmol $d^{-1}$) into the bay. Since nutrient loading is a concern in St. Louis Bay for eutrophication, understanding the role SGD plays is an important consideration for managing this environmental issue.

ACKNOWLEDGMENTS

I would like to thank my advisor, Alan Shiller, for his contribution and insight to this work. I would also like to thank my committee members, Christopher Hayes and Davin Wallace for their input into this research project. For aid in the field and in the lab, I would like to thank Melissa Gilbert, Amy Moody, Peng Ho, and Laura Whitmore. I would like to thank Virginie Sanial for useful discussion to crafting this thesis. I would also like to acknowledge the University of Southern Mississippi for the funding of this project.

TABLE OF CONTENTS

LIST OF TABLES

LIST OF ILLUSTRATIONS

LIST OF ABBREVIATIONS

| | |
|---|---|
| SGD | Submarine groundwater discharge |
| SLB | St. Louis Bay |
| MS | Mississippi Sound |
| GOM | Gulf of Mexico |
| SPM | Suspended Particulate Matter |

# CHAPTER I - INTRODUCTION

This thesis assesses the role of submarine groundwater discharge in St. Louis Bay, Mississippi. Located along the northern Gulf of Mexico, St. Louis Bay (SLB) is a semi-enclosed bay that is important to the local area for recreation and tourism. The bay is bracketed by small communities that utilize the bay for swimming, fishing and sailing. In addition, there are many residences built along the bay as well as a casino. The bay itself is seen as an attraction, but it is also important naturally as a habitat for fish and other wildlife along the banks. In 2010, approximately 8,000 young seatrout were released to seed the bay as a fishery resource (Bowman, 2010). Despite its appeal, this environment has also had water quality issues (Liu et al., 2008). Therefore, understanding how substances are introduced into the bay is important to managing it as a resource for both the general population and the natural environment.


Figure 1.1 *Map of St. Louis Bay*

## 1.2 Background

Over the last two decades, submarine groundwater discharge (SGD) has been found to be an important source of biogeochemical constituents in coastal environments (Slomp and Van Cappellen, 2004). SGD is the movement of any water into the water column across the sediment-water interface (Moore, 1999). The water that travels across this interface can consist of fresh groundwater as well as recirculated seawater, which is water that has infiltrated into subsurface sediments and subsequently reintroduced to the bottom waters. Despite returning to its original reservoir, this seawater along with groundwater flowing out can take on unique properties from the mixing zone in the sediments where redox conditions can be very different than in the receiving body of water. Globally, it is thought that the fresh component of SGD is <10% of the total SGD water flow (Burnett et al., 2003). Like rivers, SGD can carry dissolved substances into the coastal environment. Unlike rivers though, SGD cannot be readily observed. To measure this flux, chemical tracers must be used to track where and at what rate SGD flux occurs (Burnett et al., 2003).

In coastal environments, SGD can be a source of a variety of substances including nutrients and pollutants (Slomp and Van Cappellen, 2004; Burnett et al., 2003). What can be found in the aquifer that is the source of SGD, is typically carried into the water body where SGD then mixes with the bottom waters. How much SGD influences surface water depends on how well the bottom water then mixes with the water column. While SGD is considered primarily a source for many substances, water can flow both ways between the groundwater and bottom waters of the coastal environment. This mixing creates what

has been termed a “subterranean estuary” where, like a surficial estuary that is the area where freshwater and seawater meet, the subterranean estuary acts the same way for the groundwater and bottom water (Moore, 1999). Because of the chemistry that can occur in the mixing zone along with the transport of different chemical species by groundwater, SGD is an important part of coastal systems worth studying in this area.

SGD is controlled by physical factors that will impede or encourage movement of water through sediments and out to bottom waters. One of the main controls is the presence of an unconfined aquifer that serves as the source of any fresh groundwater as well as where infiltrating bottom water will permeate. Driving forces for groundwater flow include tides and currents along the bottom of the water body. Depending on the environment, SGD can move differently. Sometimes, it occurs as a very diffuse seepage along a large swath of area. In some cases, there are localized hotspots such as groundwater springs where groundwater comes in as a point source (Burnett et al., 2003). Sediment type can significantly influence SGD flow rates. Sediments with higher permeability allow for easier flow of SGD. This sediment type influence is seen especially in paleochannels. Paleochannels are the sites of old river channels which typically have coarser sediments than the areas around them. Studies of these features have shown preferential flow through the paleochannel sediments than in the area around them (Mulligan et al., 2007; Samadder et al., 2011). The bottom of the bay in this study has variable sediment compositions which could contribute to the variation in SGD (Bera, 2014).

To study groundwater in the bay, naturally occurring chemical tracers were used. Radium was used primarily and is a useful SGD tracer because of its presence naturally

in SGD which comes from enrichment while groundwater is in contact with sediments (Moore, 1996). There are four isotopes that are used specifically for investigating SGD: $^{223}$Ra, $^{224}$Ra, $^{226}$Ra and $^{228}$Ra. These isotopes are radionuclides, and they all have different half-lives (see Table 1.1). Because of the range of half-lives of different radium species, ranging from 3.6 days to 1602 years, different isotopes offer different advantages depending on the time scale one is examining. The decay provides a measure of time that can be used for aging water masses, including SGD (Moore, 2000; Moore et al., 2006). Additionally, because of the enrichment of radium in groundwater compared to other water sources for an estuary, radium can be used as a chemical tracer for SGD (Bejannin et al., 2017). By quantifying radium inputs and outputs for a defined system, a mass balance approach can be used to determine SGD flux which has been done in several studies (Charette et al., 2001; Rodellas et al., 2015; Rodellas et al., 2017; Bejannin et al., 2017). This mass balance approach was adapted for application in St. Louis Bay and is described in more detail in later sections.

While SGD is typically a major source of radium into coastal waters, radium can also be delivered via rivers, offshore sources, and diffusive fluxes from bottom sediments. For coastal waters, the main removal of radium would be the movement of water offshore and in situ decay of the radionuclide. For the long-lived species of radium, decay is considered negligible and is often ignored. However, for shorter lived species, decay constitutes a large sink of radium from the system. For this study, the short-lived Ra isotopes, $^{223}$Ra and $^{224}$Ra are used as tracers.

Table 1.2

*Half-lives of Radium Isotopes and Respective Daughter Isotopes*

| | | |
|---|---|---|
| **Ra-223** | → | **Rn-223** |
| 11.43 days | | 3.96 s |
| **Ra-224** | → | **Rn-220** |
| 3.6 days | | 55 s |
| **Ra-226** | → | **Rn-222** |
| 1602 years | | 3.8 days |
| **Ra-228** | → | **Ac-228** |
| 5.7 years | | 6.1 minutes |

Radium can be dissolved in the water column or adsorbed onto particles. The amount of desorption depends primarily on salinity, though it can be somewhat influenced by other factors such as pH (Gonneea et al., 2007). At low salinities, radium stays adsorbed onto particles and becomes desorbed as salinity increases. While most of the desorption occurs between salinities 8 and 10, desorption begins at about salinity 5 and full desorption occurs by salinity 15 (Krest et al., 1999). When measuring dissolved radium in samples less than this salinity range, adsorbed radium is not measured with the analytical procedures presently used and can affect data interpretation when comparing dissolved radium in samples at higher salinities. This distinction is particularly important when measuring delivery of radium by rivers and fresh groundwater. However, it is possible to perform desorption experiments in the laboratory to determine radium delivery from fresh sources. Desorption experiments typically involved mixing radium free seawater with a fresh sample or adding salt directly to the sample where the sample reaches full radium desorption (Gonneea et al., 2007).

In addition to radium, another mass balance was done using barium. Barium is a naturally occurring trace element that can also be enriched in groundwater. This element was used to compare to radium because it can be used as a groundwater tracer but is not subject to decay. Except for decay, the same mass balance inputs and outputs were used for barium. Like radium, barium adsorption can also be affected by salinity, so barium samples were also taken during the river desorption experiment done for radium. Existing literature was used to estimate the release of barium from bay sediments. Radon is also a useful radionuclide tracer for hotspots since it is enriched in SGD, but because of its short half-life, changes in its concentration can be strong evidence for SGD hotspots (Burnett and Dulaiova, 2003; Dulaiova et al., 2010).

From previous work on methane fluxes in St. Louis Bay, Mississippi, there seems to be a measurable amount of methane coming from the bay sediments either by advective flow of groundwater or sediment diffusion (Roberts, 2014). Having this previous information makes the bay a good place to do a groundwater study since there is likely some measurable SGD presence. The bay is relatively shallow and well mixed from wind (Martin and Camacho, 2013). Regarding the movement of water for the bay, there are two main rivers, the Jourdan and Wolf Rivers, and an opening to the Mississippi Sound. The bay is dynamic and would flush about every 15-40 days under normal conditions; however, large rain events will flush the bay even more quickly (Martin and Camacho, 2014; Veeramony and Blain, 2001). Based on preliminary sampling, there can be very large differences in overall salinity of the bay. While this variation over time can be a challenge for comparing multiple sampling trips, it also is a chance to see the effects of several different states of the bay. The bay has some characteristics which make it

well-suited for investigating submarine groundwater discharge. While many SGD studies have focused on areas that are considered either pristine or heavily influenced by human activity, St. Louis Bay is a more intermediate environment in this respect. There is some development around the bay, though it is not a heavily populated area. In this region, there is groundwater withdrawal for drinking water which can impact the aquifer composition around the bay and seawater intrudes into the aquifer (Burnett et al., 2003). Another characteristic of the bay is that is generally very shallow, meaning that the bay does not have significant stratification because of how easily it is mixed by wind. The lack of stratification means that processes along the bottom of the bay like SGD can have an impact throughout the water column.

The St. Louis Bay has also been dredged to promote waterway access to the rivers that feed into the bay. Dredging is an anthropogenic activity thought to increase SGD flux. By removing the top layers of sediment to possibly expose sediments that are more permeable to groundwater flow, dredging can promote SGD flux. Another thought is that the dredging channels can allow for lateral flow of groundwater from the walls of the channel, which increases surface area for groundwater flux and possibly a more preferential path compared to advective movement vertically through sediments (Burnett et al., 2006; Santos et al., 2008; Douglas et al., 2020). A map of the dredged channels and further discussion can be found in Section 3.3.5.

Besides just how much water is introduced by SGD, it is also important to look at what is being introduced by this flux. Radium is one flux as well as radon. For this project, nutrients, methane and barium are also being considered. In the following paragraphs, we consider the justifications for quantifying these three components.

Nutrients have been found to be more concentrated in groundwater than in rivers in some areas, and SGD can be a significant input of nutrients for many coastal systems even though SGD flux volume is typically lower than rivers (Slomp and Van Cappellen, 2004). Accounting for this input can be important for determining nutrient delivery in coastal areas. Nutrient loading and eutrophication are a concern for many coastal areas because of the detrimental effect they typically have. An overabundance of nutrients can cause algal blooms that affect light attenuation and oxygen depletion for other living things in these areas. In some areas, SGD has been suggested as a factor in the cause of harmful algal blooms (Liefer et al., 2009).

Methane is produced biologically in the sediments. Methane is from biological sources in groundwater, as the high pressure and temperature conditions needed to produce methane thermogenically are not attained in the surface (Dulaiova et al., 2010). From previous work, there is a source of methane from the bay sediments, but whether the methane is from diffusion from sediments or SGD is not entirely certain (Roberts, 2014). By comparing the total methane flux from the bottom of the bay to a calculated sediment diffusion flux, I will attempt to attribute what portion of excess methane is due to SGD.

Barium is used as an SGD indicator since it is typically enriched in the sediments where it can be dissolved in groundwater and then carried by submarine groundwater discharge (Shaw et al., 1998). Barium behaves similarly to radium in that it is adsorbed onto sediments in freshwater aquifers. Barium can be released into the groundwater, primarily when there is saline groundwater intrusion causing Ba desorption off particles at increased salinity. Shaw et al. (1998) showed that groundwater was highly enriched in

barium, much more so than in rivers. In the area they studied, the South Atlantic Bight, rivers alone could not account for the barium fluxes found in the inner shelf waters and aquifers were an important reservoir for barium.

Macro-nutrients were also chosen for study because of their importance in the environment. Nutrients are typically found to be enriched in groundwater compared to river water, thus groundwater can be an important source of nutrients even if the discharge flux is less than that of river input into the same system (Knee et al., 2016; Null et al., 2012). Nutrients are incorporated into this study to characterize potential groundwater sources and compare with river influence.

Submarine groundwater discharge has previously been studied to some extent in this region. There has been some work published about the impact of SGD in coastal water offshore from the Mississippi River outflow (Krest et al., 1999). To the east, some research has also been done in Mobile Bay looking at the relationship between harmful algal blooms and SGD (Liefer et al., 2009). There has also been a study in Mobile Bay looking at SGD and nutrient delivery into the bay (Monteil et al., 2016). From some preliminary work (Sanial et al., 2018), it has been shown that bottom waters off the coast of Mississippi have enriched radium and barium in some areas. These elements are typically enriched in groundwater, so to find these in bottom waters is a strong indicator for the presence of groundwater (Gonneea et al., 2013; Shaw et al., 1998). Submarine groundwater discharge is typically oxygen poor and higher in nutrients compared to coastal waters. The research addressing harmful algal blooms in Mobile Bay also supported a link to groundwater discharge. Large nitrate inputs were encouraging the

growth of harmful algal bloom species in the bay, Pseudo-nitzschia spp., which utilized the high nitrate conditions in a localized area (Liefer et al., 2009).

### 1.3 Study Site

St. Louis Bay, MS, has been chosen for this study for a few primary reasons:

(1) SGD in St. Louis Bay could provide useful information about how SGD behaves in this type of environment even outside of this region of the northern Gulf of Mexico. The bay is neither pristine nor heavily impacted by human activity. It is an area where groundwater is drawn from aquifers for drinking water which encourages seawater intrusion into the aquifer and groundwater movement. The bay is very shallow and is typically well-mixed, meaning groundwater impacts would likely be seen throughout the water column.

(2) Estuaries are important, complex environmental systems and SGD can be an important part of these systems depending on the area (Sadat-Noori et al., 2016);

(3) Previous work has suggested that there may be SGD entering the bay (Roberts, 2014).

St. Louis Bay, Mississippi, covers about 4000 hectares of surface area and is on average 1.3 m deep. The bay is typically well-mixed because of its shallow depth, allowing wind forcing to mix the bay (Martin and Camacho, 2013). St. Louis Bay has two rivers that flow into it, the Wolf River to the east and the Jourdan River to the west. The Wolf River discharges 22 $m^3 s^{-1}$ on average, while the Jourdan River discharges about 15 $m^3 s^{-1}$ on average (Martin and Camcho, 2013). Tides are small in amplitude within the bay and the river inputs provide much of the forcing for water movement (Veeramony and Blain, 2001). The bay has been home to several previous studies

including background study of the bay sediments and methane residence times (Bera et al., 2018; Roberts, 2014). From previous work, the bay has known pollutants including fecal coliform bacteria, nutrients and oxygen-depleting substances (Liu et al., 2008). The bay varies spatially, where near the rivers, the bay is fresher while towards the mouth of the bay, the salinity increases. From previous work (Bera, 2014), there is also data regarding the surficial sediment distribution in the bay. The east side of the bay is much sandier compared to the sediments along the north shore and towards the west side of the mouth of the bay. The variation in surficial sediments can be an important factor in preferential flow of SGD. Since sandier sediments are typically more permeable, water can flow more freely in these areas (Russoniello et al., 2013).

### 1.4 Hypotheses

The overarching hypothesis is that submarine groundwater discharge (SGD) significantly contributes to the chemical mass balance of St. Louis Bay in respect to radium, barium, methane, and nutrients. To break down this idea, there are several sub-hypotheses that will be tested also including spatial variation of SGD flux. Using the radium balance to estimate SGD flux of water, fluxes related to various chemical balances can then be calculated. While SGD volume flux will be calculated, how much water is delivered is not as important compared to what is being carried by this flux.

Regarding spatial variation across the bay, I hypothesize that spatially the input of SGD is likely to be impacted by the surficial sediment grain size along the bottom of the bay, specifically that the areas with higher sand content in the surficial sediments will have more SGD input. This hypothesis will also be tested using the information from the radon survey.

Using the information about SGD volume flux taken from the radium and barium mass balances, I hypothesize that SGD delivers a large portion of the bay's radium inventory. For barium, I hypothesize that there is a significant flux of barium from SGD. Here, I use the term 'significant' to mean there is a measurable amount of barium that is found in SGD even when accounting for the measurement uncertainty.

Using methane balance information from previous work (Roberts, 2014), I will derive an estimated methane flux from SGD. While the rivers introduce a large amount of methane to the bay, I hypothesize that methane from SGD will also be an appreciable source of methane in the bay, though it may not surpass rivers. Like the barium, I hypothesize that SGD is a significant source of nutrients for the bay. Evidence from SGD studies in other areas supports this idea and will be tested in this experiment.

Regarding nutrients and SGD flux, I hypothesize that nutrient flux via SGD will be a significant source for the bay. With the bay being moderately impacted by human activity and sewage, I hypothesize that nitrate flux will be high in SGD. With the data being collected, it is not feasible to ascertain the source of nutrients in SGD to the bay, but these could include fertilizer or wastewater.

# CHAPTER II - METHODS

## 2.1 Field Sampling

### 2.1.1 St. Louis Bay Sampling

Several field sampling trips were done. Preliminary studies were done to first determine whether SLB was a suitable site to study SGD. To do this, surface samples were taken and analyzed for possible groundwater indicators including radium, barium, and methane. Samples were also taken for alkalinity and colored dissolved organic matter (CDOM) which were initially sampled to determine if they could be used to distinguish fresh groundwater from river water in the bay.

After performing preliminary sampling, further sampling was done to collect data to use in mass balance calculations and to determine SGD nutrient fluxes. Samples were taken from a boat and the station map is below (Figure 2.1) while station locations are listed in Table 2.1. Because of how shallow SLB is, samples were taken exclusively from surface waters. These surface samples were taken over the side of the boat. In the case of the barium sample, to prevent contamination by the boat, samples were taken off the bow, facing into the direction of the water movement so that the water being sampled had not yet been in contact with the boat before sampling.


Figure 2.1 *Map of St. Louis Bay Sampling Stations*

Table 2.1

*St. Louis Bay sampling location coordinates in decimal degrees*

| Site ID | Latitude | Longitude |
|---|---|---|
| SLB-1 | 30.31433 | -89.30508 |
| SLB-2 | 30.35623 | -89.29099 |
| SLB-3 | 30.35731 | -89.32397 |
| SLB-4 | 30.34057 | -89.36111 |
| SLB-5 | 30.33693 | -89.32292 |
| SLB-6 | 30.36892 | -89.35376 |
| SLB-7 | 30.36850 | -89.35349 |
| SLB-8 | 30.36776 | -89.35329 |
| SLB-9 | 30.37479 | -89.33181 |
| SLB-10 | 30.37439 | -89.33203 |
| SLB-11 | 30.37331 | -89.33249 |

Table 2.1 (continued).

| Site ID | Latitude | Longitude |
|---|---|---|
| SLB-12 | 30.33956 | -89.33282 |
| SLB-13 | 30.33951 | -89.33182 |
| SLB-14 | 30.35069 | -89.34843 |
| SLB-15 | 30.36772 | -89.32372 |
| SLB-16 | 30.36281 | -89.34663 |
| SLB-17 | 30.33206 | -89.29561 |

### 2.1.2 River Sampling

To provide information about river inputs to the bay, samples were collected from the Wolf River (coordinates: 30.377914 N, -89.231456 W). Two radium samples were collected as part of the radium desorption experiment. From these samples, subsamples were also taken to analyze barium and nutrients. The radium samples were about 50 liters to account for the low dissolved radium concentrations found in river water. Water was collected by throwing out tubing towards the middle of the river with an anchor attached. This water was then pumped onshore. To collect a sample for dissolved radium, a 0.45 micron filter was attached in line prior to being pumped through a column containing a manganese fiber to adsorb the dissolved radium from the sample (Rama and Moore, 1996). The filtered water was then collected to determine the volume filtered. To collect the sample to measure total radium, the water was pumped onshore and collected in 20-L Cubitainers® without being filtered. Multiple Cubitainers® were used for a total sample volume of about 50 liters.

### 2.1.3 Groundwater Sampling

Groundwater samples were taken along a sandy section of the SLB shoreline (Fig. 2.2). This location was chosen given that it was accessible with sampling equipment and that the sandy sediments were conducive to the groundwater sampling method. Samples were taken using a pushpoint sampler (MHE Products). The pushpoint sampler is made of stainless steel and is 6 ft long. It is composed of two pieces: a narrow, stainless steel rod and a stainless steel tube fitting snugly over the rod. The tube has slitted openings along the bottom 5 cm and a pointed end. The slits allow for groundwater to enter and be pumped up through the steel tube during sampling while the point makes it easier to drive the sampler into the ground. To take a sample, the tube with the rod inside is driven straight down into the ground while avoiding bending the steel rod and tube. Once the sampler is at a depth where groundwater is to be sampled, the rod is removed leaving the tube in the ground. The tube then acts as a conduit to access the groundwater which can be delivered to the surface using a peristaltic pump with tubing connected to the opening at the top of the tube. After clearing bubbles from the tube and tubing used to pump water, samples can be taken. Samples were taken for barium, nutrients and radium by pumping water through the pushpoint through silicone tubing. Methane samples were not taken due to the methane analyzer being unavailable at the time of sampling.


Figure 2.2 *Map showing groundwater sampling location.*

### 2.1.4 Radon Survey

The radon survey was performed with an in-situ method using a RAD7 radon detector with RADAQUA equilibrator accessory (Dimova et al., 2009). The survey was performed in August 2018 within SLB primarily along a north-south transect (see Figure 3.8). The RAD7 (Durridge, Inc.) uses an alpha particle detector to detect decay of radon isotopes $^{220}$Rn and $^{222}$Rn by counting the decay of their polonium daughter isotopes. The instrument requires air to be pumped over the detection plate. The air carries radon and as it decays over the detection plate, the alpha particle emissions from the decay are counted. The instrument then reports the data in counts per min of radon. The RADAQUA accessory system is used together with the RAD7 and uses a water-air equilibrator to equilibrate water flowing continuously into an equilibration chamber. Air

is pumped out of the equilibration chamber and through the RAD7 instrument before being pumped back in the chamber. This closed air loop must be equilibrated with the water being pumped before readings stabilize. This system was deployed over the side of a small skiff and was equilibrated by operating it in the same location for 20 minutes until readings stabilized. From there, the boat traveled slowly (<8 kph) as the RAD7 took readings continuously. A GPS was used to track the boat's path and was matched with the RAD7 readings. Using the RAD7 Capture software, radon in water concentrations were calculated from the radon in air measurement taken in the field. The lag time of the instrument was then used to match the concentration data to its correct corresponding location.

### 2.2 In-lab experiments

To quantify SGD using a radium balance, parameters in the balance needed to be defined using controllable in-lab experiments. The two experiments performed were to provide data for two different parameters: input of radium via diffusion from surficial sediments and radium input from rivers.

#### 2.2.1 Radium Diffusion from Sediments

A radium diffusion experiment was done to determine how much radium is released into the bay by desorption from surficial sediments and subsequent diffusion into overlying bay waters. This experiment was done by taking a sediment sample from the bay and equilibrating it with a radium free sample of bay water over a 2-day incubation period. The incubation period was chosen based on data from previously published literature showing a minimal impact on sediment diffusion in longer incubations (Gonneea et al., 2008). The sediment samples were collected in August 2018. Based on

surficial sediment data available, the sediment samples were chosen from different areas of the bay with different sediment compositions (Bera, 2013). Radium-free bay water was obtained by filtering a bay water sample through two Mn fiber columns at <1 L $min^{-1}$ which would remove the radium from the water. The sediments were dried at 40°C and stored in plastic bags until use. Samples were dried to drive off water and to accurately determine the water volume used in the experiment.

To equilibrate the sediments in water, a 4-L subsample with 350 g of sediment was used in each trial. These quantities were chosen based on previous work (Dulaiova et al., 2010; Gonneea et al., 2008). Before the experiment, the samples were weighed and spread out over the bottom of three open-air, cylindrical containers so that the surface area of each sediment diffusion was determined by the area of a circle. In one sample where the sediments solidified after drying, the surface area of a cylinder was used to estimate the area interfacing with the water given that the solid sediments were cylindrical in shape. The water was then slowly poured over the sediments to minimize resuspension. The sediments were mildly agitated with the introduction of water but were almost completely settled within the first hour of the incubation. The samples were left for approximately 48 hours without disturbing the sediments to avoid sediment resuspension events. After 48 hours, the water was pumped from the containers with a peristaltic pump over a Mn fiber. The Mn fibers were then analyzed using the same procedure as the other samples collected in this study (see Section 2.3.1).

### 2.2.2 Radium Desorption from SPM from Rivers

This experiment was done to look at how much radium is available for desorption from suspended particulate matter (SPM) in the rivers that flowed into the study site. At

low salinities, radium is not entirely conservative because radium adsorbs to SPM. As salinity increases, radium is desorbed from these particles until near complete desorption at higher salinities (Gonneea et al., 2007). Thus, it is important to account for this adsorbed radium since it is an additional input of radium into the bay along with the dissolved fraction which was measured directly.

To determine the dissolved and desorbable radium fractions in the rivers, two samples were taken from a site along the Wolf River. Because of their similar watershed environments and climate, the Jourdan and Wolf rivers were assumed to have the same radium concentrations. The samples were taken by using a peristaltic pump. The first sample for dissolved radium was filtered using a .45-µm filter and filtered over a Mn fiber as described in Section 2.1.2. The second river sample was collected unfiltered in 20-L Cubitainers and brought back to the lab.

In the lab, the second sample was combined in another 100-L container. Sodium chloride salt was then added to this sample to raise the salinity from 0 to 30. By raising the salinity, the adsorbed radium would then desorb and go into solution where it could be measured to determine the desorbable fraction. The sample was left for 24 hours to allow for full desorption. To ensure that the sample stayed mixed, a pump was used to bring water from the bottom of the container to the top continuously. After 24 hours, the water was then filtered through a Mn fiber at about 1 L $min^{-1}$. The sample was then analyzed using the same procedure used for the rest of the sample collected in this project (see Section 2.3.1).

## 2.3 Sample Analysis

### 2.3.1 Radium

$^{223}$Ra and $^{224}$Ra were measured using a RaDeCC system (Scientific Computer Instruments) via established methods described in Moore and Arnold (1996). The RaDeCC counts the radium decay daughters, $^{220}$Rn and $^{219}$Rn using an alpha scintillation counter. With the count data, the activity of the radium isotopes, $^{223}$Ra and $^{224}$Ra, can then be calculated via the decay of the daughters. Samples were collected by filtering sample water through a column that holds a manganese-coated fiber. The radium adsorbs onto the fiber. This fiber is then rinsed with distilled water and attached to the instrument. During the analysis, helium is first pumped through the Mn fiber column and then through the instrument in a closed loop. The He gas continuously pumps through the sample, carrying the Rn daughters to the detection plate. To account for the background radium in the instrument, background runs are done immediately prior to running a sample. In addition, the instrument efficiency is also monitored using a Mn fiber standard to determine how efficient the instrument is at the time of the sample run since the efficiency can vary over time (Garcia-Solsona et al., 2008).

### 2.3.2 Methane

Dissolved methane was measured from surface samples in the bay. Dissolved methane was determined using headspace equilibration and analysis of the headspace gas by cavity ringdown spectroscopy (CRDS; Picarro G2301) following the method of Roberts and Shiller (2015). Briefly, this method involves collecting water in a 140-mL syringe, equilibrating the 70-mL of the water sample with 70-mL of methane-free (“zero”) air, and then carefully transferring the equilibrated headspace to the CRDS for

analysis. The concentration of methane in the water can then be calculated using air/water equilibrium equation of Wiesenburg and Guinasso (1979). Calibration of the CRDS was accomplished by measuring both zero air and a 5 ppb methane standard. As described in Roberts and Shiller (2015), the relative precision of this method is typically 4% and it has a detection limit of 0.13 nM. Based on the previous work of Roberts (2014) in St. Louis Bay, I expected concentrations of dissolved methane in the range 0 - 400 nM depending on location in the bay. Because samples were analyzed in the lab roughly half a day after collection, syringes of water samples for analysis were kept in a dark cooler slightly above freezing to minimize microbial activity that might alter dissolved methane concentrations. Because dissolved methane in bay waters appears to come largely from the sediments, methanogenesis and methanotrophy in the water samples will likely occur at a low enough rate relative to the dissolved concentrations that samples were not poisoned (Roberts, 2014).

### 2.3.3 Barium

Barium samples are filtered via acid cleaned 25 mm 0.45 µm filters. After returning to the lab, samples are acidified to pH < 2 using ultrapure hydrochloric acid. Using an inductively coupled plasma mass spectrometer, barium was analyzed using an isotope dilution method. The isotope dilution method is described in Joung and Shiller (2014). Samples were spiked with a known amount of $^{135}$Ba. This spike is used to determine the $^{138}$Ba in the sample using the isotope ratio measured by the instrument. Since $^{135}$Ba is a known amount and the natural and enriched spike ratios are also known, the $^{138}$Ba can then be determined from this information. For checking the accuracy of the run, a certified reference was also used.

### 2.3.4 Nutrients

Nutrient (nitrate, phosphate, nitrite, and ammonium) samples were filtered using a 25mm 0.45 µm filter then frozen before analysis using a Seal Auto Analyzer 3 (AA3). Concentrations were determined using a standard curve and first order regression statistics. To evaluate the precision of the analysis, a sample duplicate was run every ten samples during the analysis. To check the accuracy of the standards used to build the standard curve, an initial calibration verification (ICV) standard was also used each run. In addition to preparing standard solutions from a primary standard, the ICV was a set of standards prepared using a different source of each respective nutrient. Because the samples being analyzed had different salinities, a matrix-matched set of standards were prepared and run as samples to determine how salinity would affect the concentration results. Salinity did not have a significant effect on the sample concentrations. All reagents were prepared per methods described in the Seal instrument manual provided with the AA3. For this project, the following methods were used:

- Nitrate/nitrite determination: Standard nitrate/nitrite determination per ISO standard (source: Seal Analytics, AA3 manual)
- Ammonium determination: Indophenol-blue method (Aminot et al., 1997)
- Phosphate determination: Murphy and Riley method (source: Seal Analytics, AA3 manual)
- Silica determination: Adapted from Grasshoff et al., 1983

# CHAPTER III – RESULTS AND DISCUSSION

## 3.1 Results from field sampling of St. Louis Bay

Throughout the several sampling trips to St. Louis Bay, salinity ranged from 0 to 21.4. Figure 3.1 shows the salinity distributions from each sampling trip. Salinity was lower farther north in the bay and increased moving south towards the Mississippi Sound. The data gathered during the August 2018 sampling trip was used to build the radium and barium mass balances. Maps showing the distribution of $^{224}$Ra and $^{223}$Ra within SLB are shown in Figures 3.2 and 3.3, respectively. Radium was generally higher when very close to the edge of the bay and at SLB-5 (centered in red area in Figure 3.2E). $^{224}$Ra varied from about 10 to 120 dpm 100-L$^{-1}$ throughout all sampling trips. $^{223}$Ra varied from about 0.5 to 10 dpm 100-L$^{-1}$. For a full table of the data collected in this study, see Table A.1 in Appendix A.

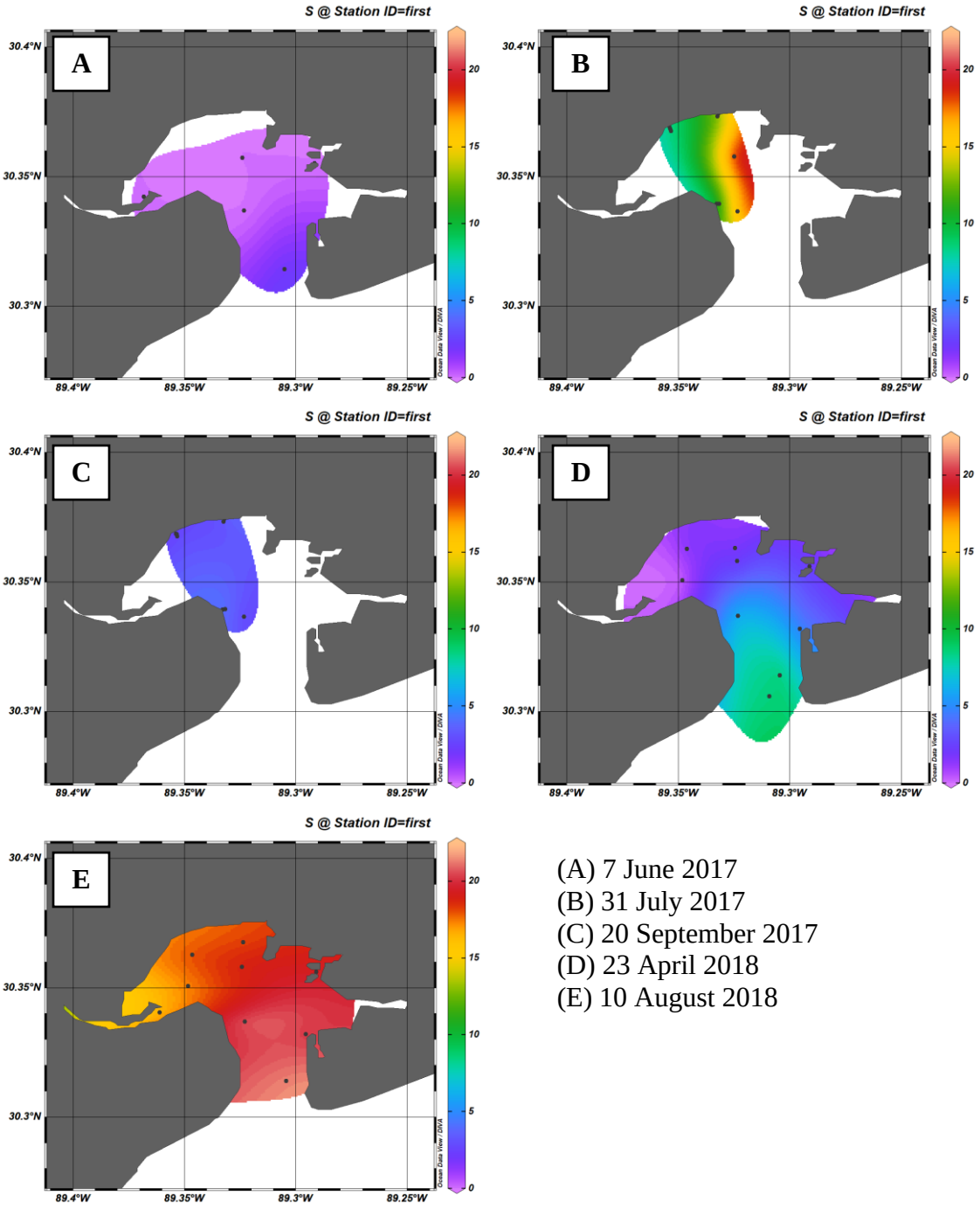


(A) 7 June 2017
(B) 31 July 2017
(C) 20 September 2017
(D) 23 April 2018
(E) 10 August 2018

Figure 3.1 *Map of salinity distribution from each SLB sampling trip*

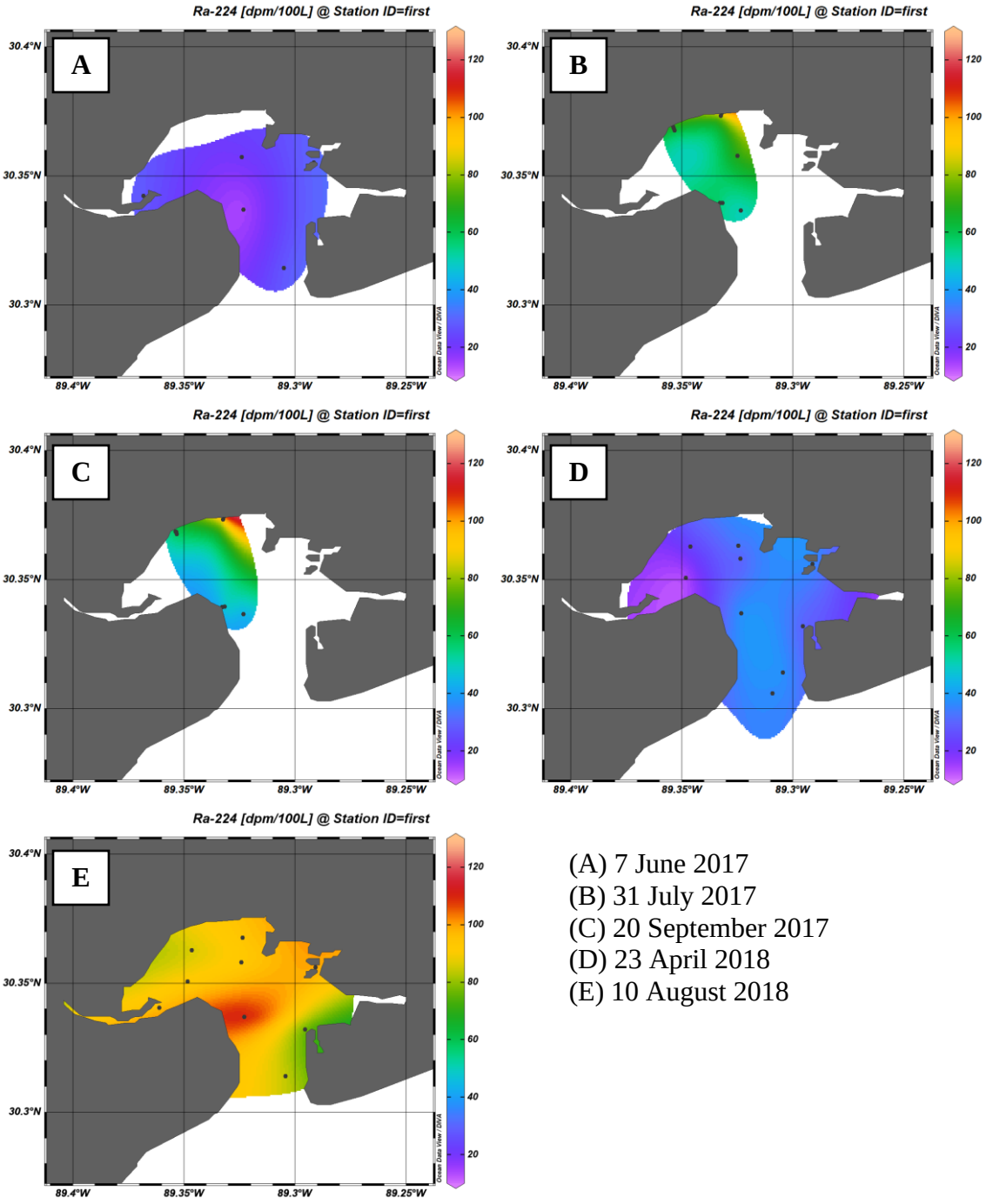


(A) 7 June 2017
(B) 31 July 2017
(C) 20 September 2017
(D) 23 April 2018
(E) 10 August 2018

Figure 3.2 *Map of* $^{224}$*Ra distribution from each SLB sampling trip*

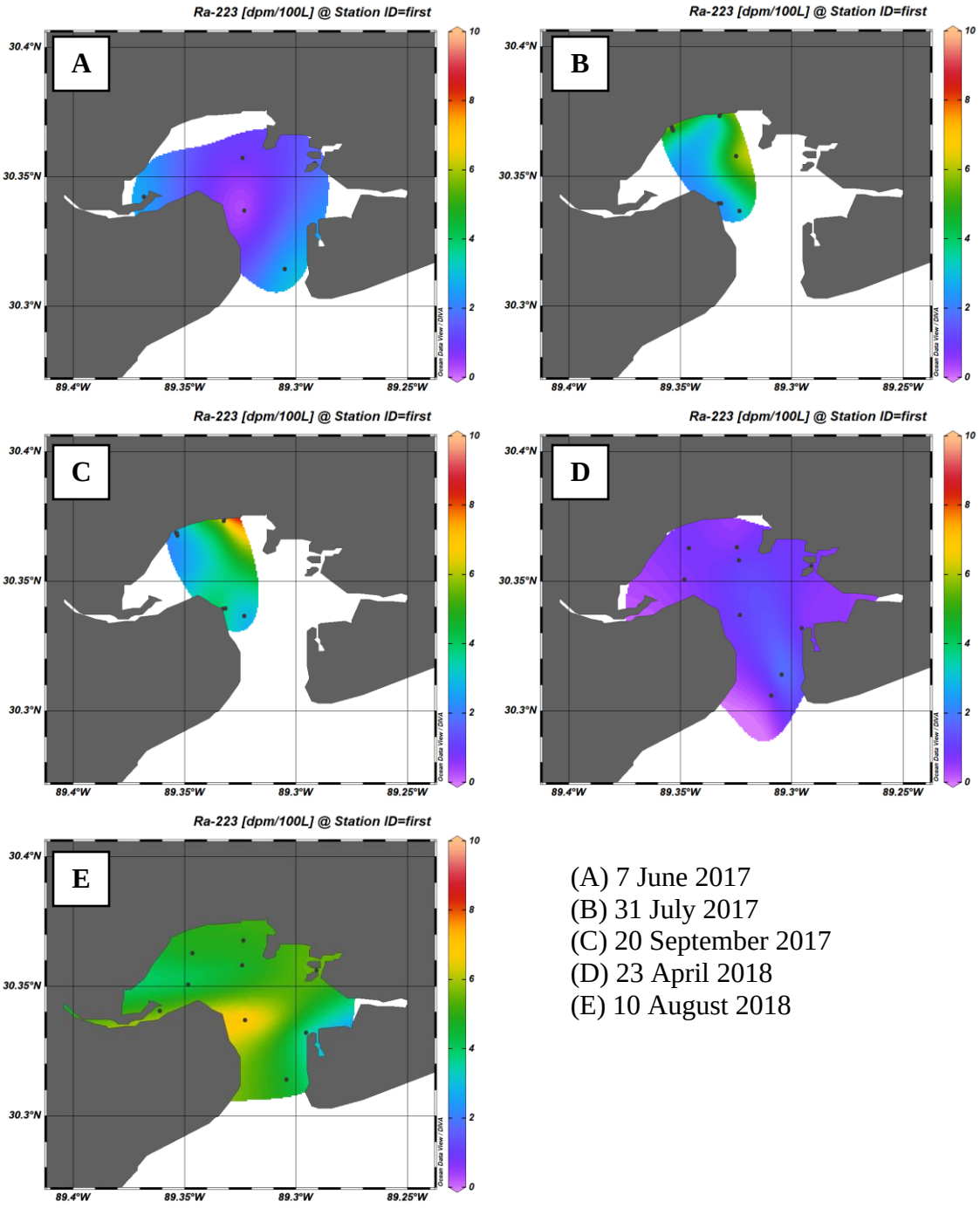


(A) 7 June 2017
(B) 31 July 2017
(C) 20 September 2017
(D) 23 April 2018
(E) 10 August 2018

Figure 3.3 *Map of $^{223}$Ra distribution from each SLB sampling trip*

### 3.2 Residence Time and Water Age

Given that the radium isotopes used in this study are relatively short-lived, with half lives in days, the residence time of SLB waters must be considered. Residence time

is the time it takes for a water parcel or chemical substance to leave an existing reservoir (Monsen et al., 2002). In this context, residence time of the water in the bay is the mean lifetime of the water in the bay before exiting to the Mississippi Sound. With the entire St. Louis Bay being considered the reservoir in the box model used here, it is assumed that it is generally uniform in concentration of the tracer being used. From Martin and Camacho (2013), the residence time of the bay under average river discharge conditions is somewhere around 38 days, though abrupt rain events can quickly flush out the bay within a few days (Veeramony and Blain, 2001). This idea of periodic, rapid flushing seems to be supported by the variability in salinity seen in the bay during sampling trips, where salinities ranged from 0 to 21.4 over the same area. Assuming a lack of major flushing events, the residence time here is the equivalent of about four half-lives of $^{223}$Ra and 10 half-lives of $^{224}$Ra. Under these conditions, it is possible that much of the radium decays before water leaves the bay. A caveat in the discussion below is that the system needs to have been at steady state at least for the flushing time of bay during any given sampling trip.

To characterize the exchange between Mississippi Sound and St. Louis Bay used in the excess radium calculation, water age must be determined. Water age is the time a parcel of water has spent in an estuary since entering from a specified boundary (Monsen et al., 2002). Apparent water age can be determined using a $^{224}$Ra/$^{223}$Ra activity ratios (AR) of surface water and groundwater samples, according to the following equation (Moore et al., 2006):

$$F\left(\frac{^{224}Ra}{^{223}Ra}\right) = I\left(\frac{^{224}Ra}{^{223}Ra}\right) * \left(\frac{\lambda_{224} + \frac{1}{\tau}}{\lambda_{223} + \frac{1}{\tau}}\right)$$

In this equation, $F\left(\frac{^{224}Ra}{^{223}Ra}\right)$ is the radium activity ratio of the radium input which is assumed to be dominated by SGD and $I\left(\frac{^{224}Ra}{^{223}Ra}\right)$ is the AR of the radium inventory of surface waters in this case. The decay constant of the respective radium isotope is denoted by λ. The water age is represented by τ, which will be referred to as $T_w$ from here on to align with the variables used in this study. This equation assumes a continuous input of groundwater and is considered suitable for estuaries according the authors. After substituting the $T_w$ term for τ and solving for the water age, the equation can be rewritten as follows:

$$T_w = \frac{F\left(\frac{^{224}Ra}{^{223}Ra}\right) - I\left(\frac{^{224}Ra}{^{223}Ra}\right)}{I\left(\frac{^{224}Ra}{^{223}Ra}\right)\lambda_{224} - F\left(\frac{^{224}Ra}{^{223}Ra}\right)\lambda_{223}}$$

The water age can then be used in the equation Section 2.4.1. It should be noted that the original equation used in Moore et al. (2006) used the ratio of $^{224}$Ra to $^{228}$Ra. However, when water age is on the scale of weeks, $^{223}$Ra can be used instead of $^{228}$Ra according to the authors. If water age was much higher, such as on the scale of months as in shelf waters, the $^{223}$Ra half-life would be too short compared to the half-life of $^{228}$Ra which is 5.7 years compared to the 11 days of $^{223}$Ra (Moore et al., 2006). Using this method, the average water age of SLB surface waters was 19.8 days.

**3.3 SGD Flux**

To calculate SGD water volume flux and derive additional chemical fluxes from this information, a mass balance was used. Assuming SLB is under steady-state

conditions, the sum of the inputs of the tracer of interest (i.e. $^{224}$Ra, $^{223}$Ra, Ba) equals the sum of the outputs where the amount of the respective tracer is constant in St. Louis Bay.

Below is a figure describing the inputs and outputs of radium in the bay. Of interest in this figure is the SGD input which was not directly measured. By constraining the other inputs and outputs, whatever amount of the tracer is unaccounted is assumed to be contributed by SGD. The following sections detail how these balances were built and compare the values found in this study with existing literature.

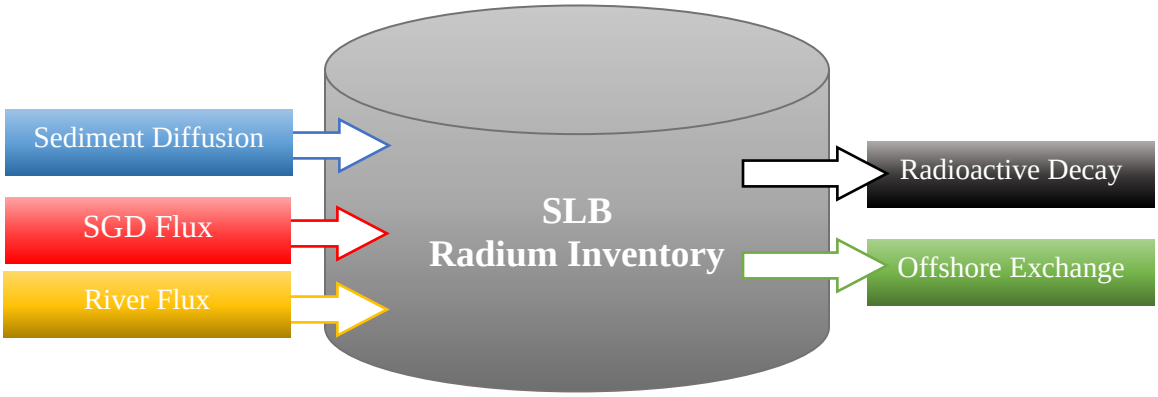


Figure 3.4 *Radium box model diagram*

### 3.3.2 Results from radium river desorption experiment

To determine the radium delivery from the rivers that empty into St. Louis Bay, information was needed regarding the adsorbed radium fraction. Fresh water from rivers with low salinity has a significant amount of radium that is adsorbed onto the fluvial SPM. As that water mixes with saline waters in an estuary, desorption of radium begins to occur. Most Ra desorption occurs between salinities 5 and 15 (Krest et al., 1999). Using the river water samples taken from the Wolf River, it was found that about 40% of the radium in the river water was adsorbed. To get the adsorbed fraction, the radium

activity in the river sample taken directly from the river was compared to the radium activities found in the in-lab experiment. In the Wolf River sample, radium activity was 13 dpm $100L^{-1}$ for $^{224}Ra$ and 0.2 dpm $100L^{-1}$ for $^{223}Ra$. After increasing the salinity in the river sample and allowing time for the adsorbed radium to release into a dissolved form, the total radium activity was 21 dpm $100L^{-1}$ for $^{224}Ra$ and 1.5 dpm $100L^{-1}$ for $^{223}Ra$. In a similar experiment, Krest et al. (1999) found that 33-39% of the short-lived Ra was adsorbed onto SPM in the Mississippi and Atchafalaya Rivers. In the mass balance, the total radium activity from dissolved and adsorbed radium in the river water was used since the adsorbed fraction would shift to the dissolved state once entering SLB.

Radium activity and barium concentration were assumed to be the same between the Wolf and Jourdan Rivers which enter SLB. Additionally, because river discharge data was not available for the Jourdan River, the Wolf River discharge data was used to estimate the Jourdan River discharge using the watershed areas of each river. The Wolf River watershed covers approximately 788 $km^2$ and the Jourdan River watershed 545 $km^2$ (Martin and Camacho, 2013). Given that the Jourdan River watershed is about 69.2% the size of the Wolf River watershed, the discharge data from the Wolf River was scaled to the Jourdan River by that proportion. Using this method, the approximate river discharge of the Jourdan River at the time of sampling was 3.8 $m^3\ s^{-1}$ given that the Wolf River discharge was 5.4 $m^3\ s^{-1}$. These values were then added together to determine the total river water volume flux used in the mass balance calculations (see Table 3.1).

The river discharge rate for the Wolf River was determined by averaging the discharge rate of the day that the St. Louis Bay was sampled. Figure 3.7 shows the river discharge for the Wolf River from July 21, 2018 to August 12, 2018. This time period

was used here based on the residence time of the bay to compare the river discharge rates since rapid flushing events can greatly impact the conditions in the bay, it was important to evaluate the river conditions leading up to the August sampling (Martin and Camacho, 2014; Veeramony and Blain, 2001). The average annual river discharge for the Wolf River is 22 $m^3 s^{-1}$ (Martin and Camacho, 2013). In the time leading up to the sampling date, river conditions were generally below average with a high of 28 $m^3 s^{-1}$ and a low of 2 $m^3 s^{-1}$ where the average river flow on the date of sampling was 5 $m^3 s^{-1}$ (area shaded in grey).

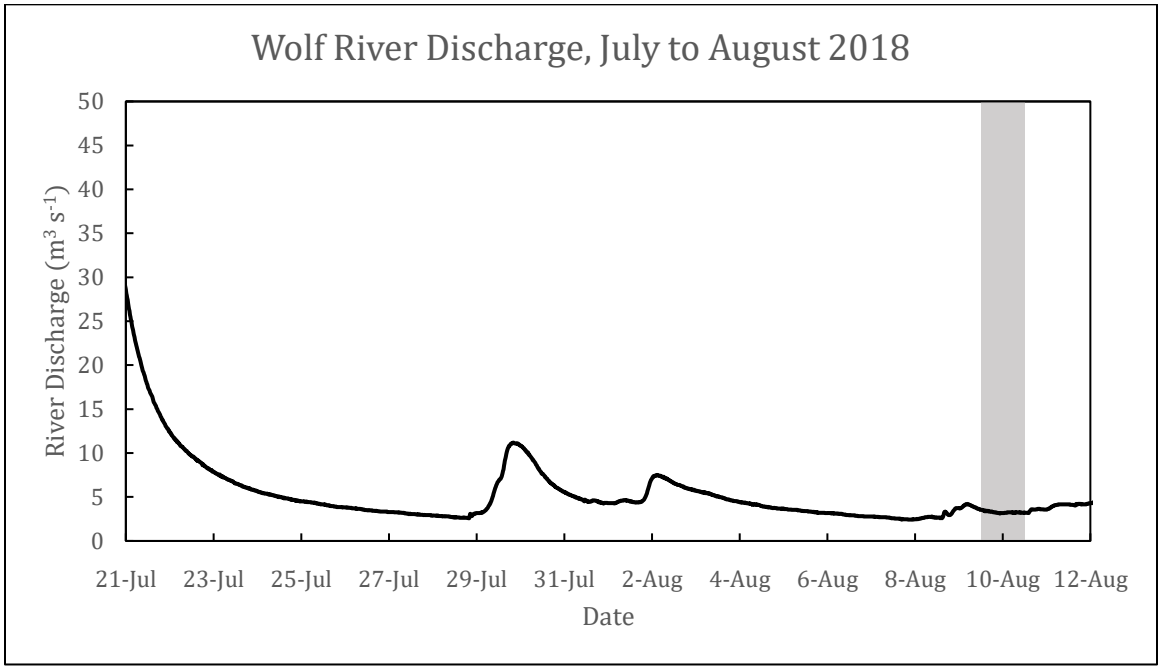


Figure 3.5 *Graph of Wolf River discharge for August 2018*

Note: River discharge data retrieved from the USGS National Water Information System. The shaded area in the graph represents the day sampling occurred, showing that no abrupt discharge changes occurred in the week before sampling.

Since the river samples were not taken at the same exact time as the samples within the bay, it is taken as an assumption that the radium concentration in the river was

relatively constant during the season. Given that the rivers were 53% of the input of barium into the bay, variability in the concentration could introduce a significant amount of uncertainty to the Ba-derived SGD water volume flux. However, variation of Ba and Ra concentrations in the rivers was not addressed in this study, so this possible source of uncertainty was not quantified. Based on previous literature, barium river concentrations have been shown to vary seasonally though the exact mechanisms that cause this change are difficult to attribute to any one cause (Shiller, 1997; Colbert and McManus, 2005). Since the mass balance built in this study was constrained to represent one time period, it's assumed that Ba delivery did not change during the approximately two-month sampling period used to collect the mass balance data. Since it was found that the rivers contribute a relatively low amount of Ra into the bay (2% and 0.5% for $^{224}$Ra and $^{223}$Ra respectively), variation in the river concentrations of these tracers would not significantly impact the overall mass balance of these tracers used in this study. Because of this relatively low contribution, errors associated with the river input of Ra had little to no impact on the SGD values calculated from the mass balance. It was assumed that the radium in the rivers went through near complete desorption once mixed with the bay. This assumption is supported by the average salinity in the bay being 19 during sampling, whereas most radium desorption takes place between salinities 5 and 15.

In regard to the uncertainty of these measurements, it's important to note that river discharge can vary and change rapidly in response to rain events. While the sampling period here did not include one of these events, variation in the river discharge could significantly impact the barium mass balance since it was such a major component of the mass balance. For instance, if the mean flow river discharge rate, $3.34 \cdot 10^6$ m$^3$ d$^{-1}$,

was used instead, this would have not significantly impacted the radium balances since the new calculated values would still be within the uncertainty of the final values. However, for the barium mass balance, this adjustment would have created a negative value for the excess barium and a negative SGD flux value. This calculation shows the importance of having an accurate river discharge determination. It should be noted that even if the river had been under more average river discharge conditions at the time of sampling, higher tracer delivery from higher discharge should also increase the tracer inventory in the bay, so the mass balance would still reasonably reflect the actual environmental conditions.

### 3.3.3 Results from radium sediment diffusion experiment

To determine the rate of radium diffusion from submerged sediments in St. Louis Bay, an in-lab incubation of SLB sediment samples was performed. The following equation was used to calculate sediment diffusion ($K_{Ra\text{-}diff}$).

$$K_{Ra-diff} = \quad Ra_{SED} \times \frac{V_{exp}}{t_{exp} \times A_{exp}}$$

$Ra_{SED}$ is the radium activity of the water that was pumped out of the incubation containers. $V_{exp}$, $A_{exp}$, and $t_{exp}$ are all values measured during the in-lab experiment for volume, area, and time respectively. The volume used was the water volume incubated (4L). The area refers to the surface area of the sediment samples exposed to the incubated water in $m^2$. The samples were incubated in cylindrical containers, so the area of circle formula was used to determine the surface area of the sediments. The time was the length of the incubation which was about 48 hours. The time was measured for each incubation from when the water was delivered to the incubation container to when the water began

to be pumped out expressed in hours and minutes. The incubation times were converted to days for the diffusion calculation so that the final units for $K_{Ra\text{-}diff}$ are in dpm $d^{-1}$ $m^{-2}$. Three incubations were done and the average sediment diffusion rate for St. Louis Bay was 170 dpm $m^{-2}$ $d^{-1}$ for $^{224}Ra$ and 5.5 dpm $m^{-2}$ $d^{-1}$ for $^{223}Ra$. Tables 3.1 and 3.2 show the data collected from the three incubations for $^{224}Ra$ and $^{223}Ra$ respectively. Among the three incubations, the sediment diffusion rates of radium varied over an order of magnitude. This variation is primarily attributed to the sediment grain size of the different sediment samples. To account for variation in grain size variation in surficial sediments in the bay, sediment samples were taken from different areas in the bay that have been shown to have varying grain size distributions (Bera, 2014). Sample 2 referred to in the tables for the sediment incubations (Tables 3.1, 3.2) had the highest fine-grained sediment composition based on the surficial sediment map of the area. To represent the sediment diffusion rate for the bay, the samples were averaged to show the contribution of variation of sediment size on sediment diffusion in SLB.

Table 3.1

*Sediment Incubation Data for $^{224}Ra$*

| Experimental Value | Sample 1 | Sample 2 | Sample 3 | Units |
|---|---|---|---|---|
| Sediment Surface Area | 507 | 117 | 507 | $cm^2$ |
| Sediment Surface Area | 0.0507 | 0.0117 | 0.0507 | $m^2$ |
| Incubation Time | 2.03 | 2.02 | 2.04 | d |
| Incubated Water Volume | 4.0 | 4.0 | 4.0 | L |
| $^{224}Ra$ Activity | 44 | 239 | 223 | dpm $100L^{-1}$ |
| Sediment Diffusion Rate | 17 | 407 | 86 | dpm $d^{-1}$ $m^{-2}$ |

Table 3.2

*Sediment Incubation Data for $^{223}Ra$*

| Experimental Value | Sample 1 | Sample 2 | Sample 3 | Units |
|---|---|---|---|---|
| Sediment Surface Area | 507 | 117 | 507 | $cm^2$ |
| Sediment Surface Area | 0.0507 | 0.0117 | 0.0507 | $m^2$ |
| Incubation Time | 2.03 | 2.02 | 2.04 | d |
| Incubated Water Volume | 4.0 | 4.0 | 4.0 | L |
| $^{223}Ra$ Activity | 2 | 7 | 10 | dpm $100L^{-1}$ |
| Sediment Diffusion Rate | 1 | 12 | 4 | dpm $d^{-1}$ $m^{-2}$ |

### 3.3.4 Mass Balance Approach

Based on the mass balance approach described in Section 3.2, the following equation was used to quantify the mass balance fluxes and rearranged to solve for the radium that would be attributed to SGD (Charette et al., 2001; Rodellas et al., 2017; Gonneea et al., 2007):

$$Ra_{ex} = \left[\frac{\left(\ Ra_{SLB} - \ Ra_{MS}\right) \times V_{SLB}}{T_W}\right] + [Ra_{SLB} \times V_{SLB} \times \lambda_{Ra}]$$

$$- \left[\ Ra_R \times F_R\right] - \left[K_{Ra-diff} \times A_{SLB}\right]$$

The purpose of this equation is to determine the flux of excess radium into the bay from SGD which is represented by $Ra_{ex}$. In other words, the radium flux that is not accounted for by other known inputs and outputs is then attributed to SGD. In this equation, $Ra_{SLB}$ is the average Ra activity for surface waters in St. Louis Bay. A mass balance was built for both $^{223}Ra$ and $^{224}Ra$. $V_{SLB}$ is the volume of the bay which is $5.69 \cdot 10^7$ $m^3$ and $A_{SLB}$ is the surface area which is $3.98 \cdot 10^7$ $m^2$. These values were taken from existing literature (Martin and Camacho, 2013). $Ra_R$ is the radium activity measured in

the rivers. This term includes both dissolved and adsorbed radium as total radium which was determined by an in-lab radium desorption experiment. Determining the total amount of radium in the river samples was necessary because the salinity of the river water was too low for significant radium desorption (S = 0). Once this water flowed in into the SLB, desorption of Ra from SPM would then cause the initially adsorbed radium to be measured in the mass balance since the radium measurement technique was for dissolved radium. The results from this experiment are described in more detail later in this paper (see Section 3.3.2.2). $T_w$ is the average apparent water age for SLB which has been was calculated using data collected from this study (see Section 3.2). $F_R$ is the water flux from the rivers which was based on the reported Wolf River discharge (USGS) and our proportional estimate of the Jourdan River discharge (Sec. 3.3.3). The diffusion rate of radium from sediments in the bay is described by $K_{Ra\text{-}diff}$ which is expressed in dpm $d^{-1}$ $m^{-2}$. This value was determined in the in-lab sediment diffusion experiment which was then scaled for the area of the bay, $A_{SLB}$.

In addition to the mass balance calculations for $^{223}Ra$ and $^{224}Ra$, a barium mass balance for SLB was also derived using the Ra mass balance as a guide:

$$Ba_{ex} = \left[\frac{\left(Ba_{SLB} - Ba_{MS}\right) \times V_{SLB}}{T_W}\right] - \left[Ba_R \times F_R\right] - \left[K_{Ba-diff} \times A_{SLB}\right]$$

In this equation, the decay term is removed because barium is not radioactive. Additionally, because a sediment diffusion experiment was not done for barium, estimates of barium diffusion rates ($K_{Ba\text{-}diff}$) were taken from previously published literature (Fiket et al., 2017). To build this mass balance, it is assumed that barium has similar sources and sinks as radium except for decay. The sources for barium are SGD,

sediment diffusion, and rivers. The sink of barium is exchange with the sound, which is a net removal of barium.

These mass balance approaches are very similar regarding the sources and sinks of radium and barium. While the mass balance equation used was not originally used for Ba, the same assumptions are made for this mass balance, including that Ba is in a steady state within St. Louis Bay. Table 3.3 provides a summary of the variables used in these equations for the radium and barium mass balances.

To determine the Ra activity and Ba concentration values for the bay in this table, samples were taken throughout SLB and the values were averaged to determine an average Ra and Ba quantity in the bay waters. The values for the Mississippi Sound were determined from samples taken in the Sound during the Rn survey trip. The Ba and Ra values for the river input were measured from a sample from the Wolf River. The river discharge value provided in the table is the sum of the Wolf River discharge and the estimated Jourdan River discharge averaged from USGS river discharge data for the day of sampling. The groundwater Ra activities and Ba concentration were taken from a groundwater sample as described in Section 2.1.3. This is sample GW-1 in Table A.1 in Appendix A.

Sediment diffusion was found to be the major source of radium in the bay. SGD was a moderate source with very little coming from the rivers. Radioactive decay was the major sink for radium, and more for $^{224}$Ra. Since $^{224}$Ra has a shorter half-life than $^{223}$Ra, it makes sense that decay would be a larger source of radium depletion in the bay. Figures 3.6 and 3.7 show the relative amounts of each input and output of radium in SLB.

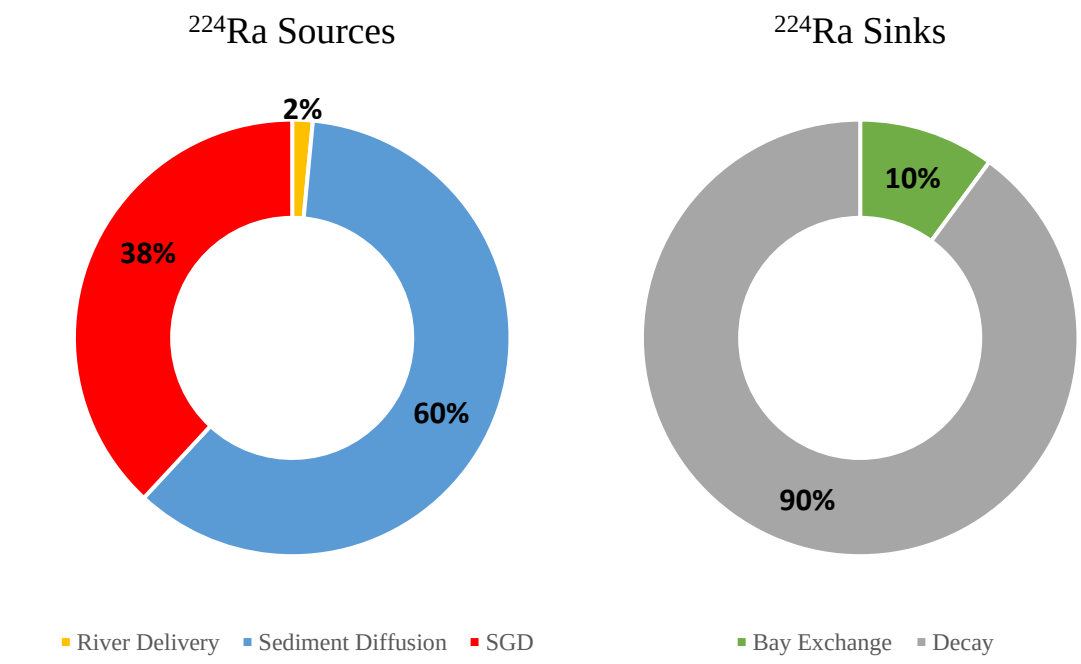


Figure 3.6 *224Ra sources and sinks in SLB*

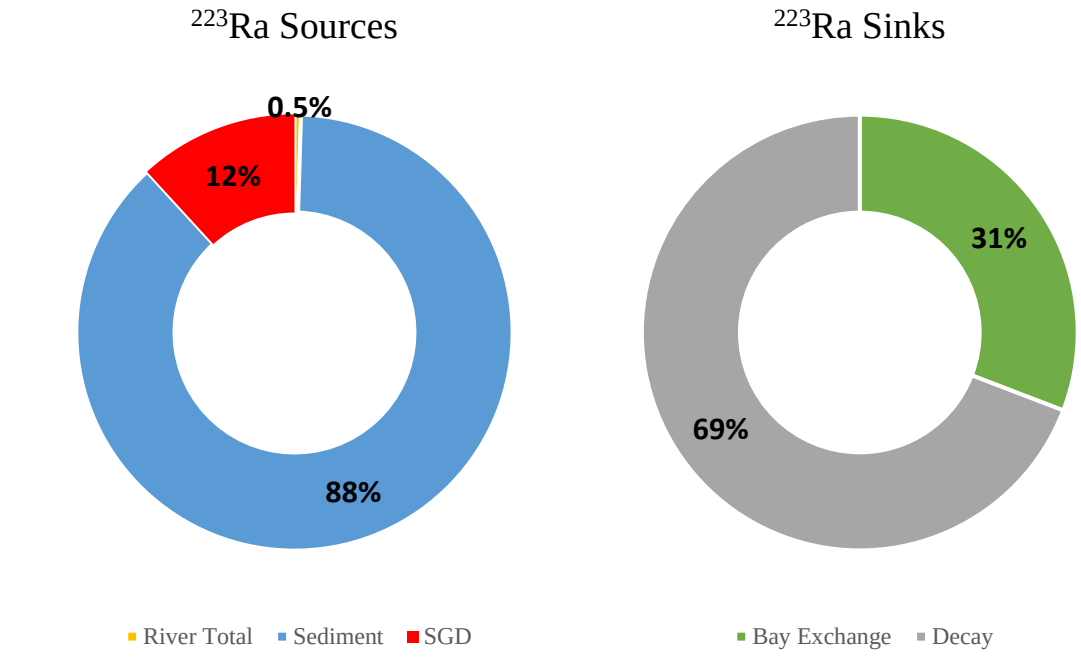


Figure 3.7 *223Ra sources and sinks in SLB*

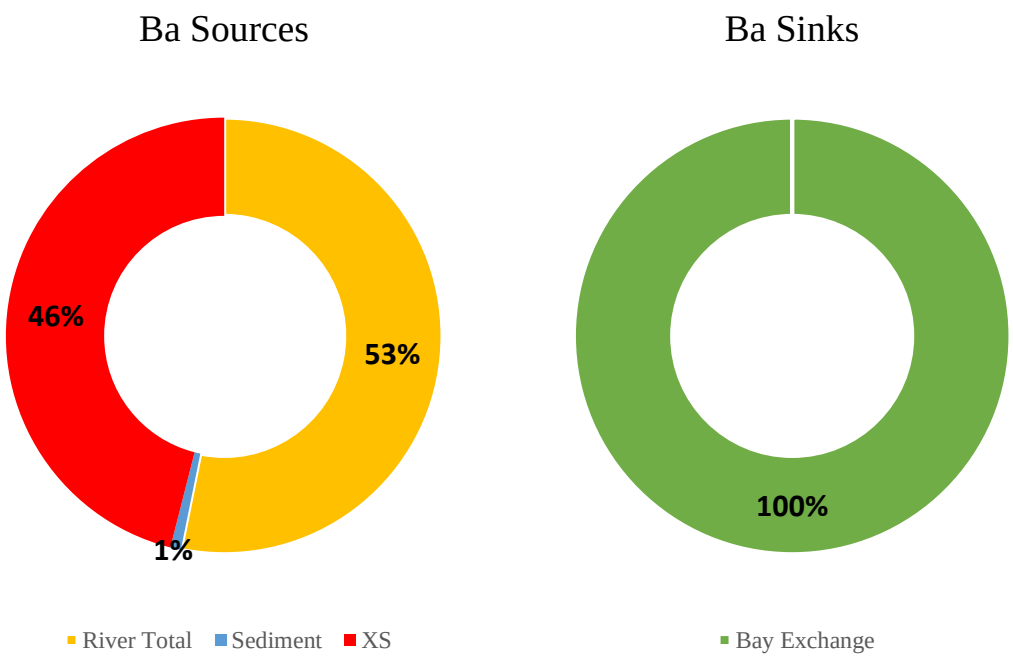


Figure 3.8 *Ba sources and sinks in SLB*

Once the mass balance equations were solved for the respective excess amount, an SGD water flux ($F_{SGD}$) could then be calculated using the following equation:

$$F_{SGD} = \frac{Ra_{ex}}{Ra_{GW}}$$

The groundwater endmember activity or concentration is needed to perform this step ($Ra_{GW}$). Using this equation, the SGD flux for the bay was found to be $9.7 \cdot 10^5$ ($^{224}$Ra), $2.7 \cdot 10^5$ ($^{223}$Ra), and $3.5 \cdot 10^5$ (Ba) $m^3\ d^{-1}$ using the three different mass balance approaches. While these amounts are not identical, they are within the same order of magnitude with the $^{224}$Ra SGD flux value being about three times greater than the other two fluxes. Using these values, the average SGD flux for the bay at the time of sampling was $5.3 \cdot 10^5\ m^3\ d^{-1}$.

While several sampling trips were done during this study, a mass balance was built only for the August 2018 trip. The groundwater and river data were taken during this period and that sampling was not done during other SLB sampling trips. Based on evidence from Gonneea et al. (2013), groundwater endmember radium concentrations can change over time so an endmember determination should be done at the same time as sampling the bay. In other words, the mass balances built are snapshots in time and extrapolating conditions past the late summer 2018 period would include large amounts of uncertainty based on evidence from other published literature. To account for uncertainty within this mass balance, error was propagated for values where an uncertainty range could be determined.

Table 3.3

*Summary table of radium and barium mass balance terms*

| Term | Description | $^{224}$Ra | $^{223}$Ra | Ba | Units |
|---|---|---|---|---|---|
| $V_{SLB}$ | Water volume of the bay[1] | | $5.69 \cdot 10^7$ | | $m^3$ |
| $A_{SLB}$ | Area of the bay[1] | | $3.98 \cdot 10^7$ | | $m^2$ |
| $T_w$ | Apparent water age | | 20 | | d |
| $Ra_{SLB}$ | Ra activity in the bay | 93 ± 12 | 5.0 ± 1.1 | | dpm $100L^{-1}$ |
| $Ba_{SLB}$ | Ba concentration in the bay | | | 504 ± 17 | nM |
| $Ra_{MS}$ | Ra activity in Mississippi Sound | 54 | 2.3 | | dpm $100L^{-1}$ |
| $Ba_{MS}$ | Ba concentration in Mississippi Sound | | | 336 | nM |
| $\lambda_{Ra}$ | Ra decay constant | 0.19 | 0.061 | | $d^{-1}$ |
| $Ra_R$ | Ra activity in the rivers | 21.4 | 0.2 | | dpm $100L^{-1}$ |

Table 3.3 (continued).

| Term | Description | $^{224}$Ra | $^{223}$Ra | Ba | Units |
|---|---|---|---|---|---|
| $Ba_R$ | Ba concentration in the rivers | | | 323 | nM |
| $F_R$ | River discharge[2] | | $7.95 \cdot 10^5$ | | $m^3\ d^{-1}$ |
| $K_{Ra\text{-}Diff}$ | Ra diffusion from sediments | 170 ± 85 | 5 ± 2.5 | | dpm $m^{-2}\ d^{-1}$ |
| $K_{Ba\text{-}Diff}$ | Ba diffusion from sediments[3] | | | 94 | nmol $m^{-2}\ d^{-1}$ |
| $Ra_{SGD}$ | Ra activity of groundwater | 440 | 10 | | dpm $100L^{-1}$ |
| $Ba_{SGD}$ | Ba concentration of groundwater | | | 641 | nM |
| $Ra_{ex}$ | Excess Ra flux | $4.3 \pm 3.7 \cdot 10^9$ | $2.9 \pm 12.5 \cdot 10^8$ | | dpm $d^{-1}$ |
| $Ba_{ex}$ | Excess Ba flux | | | $2.2 \pm 0.5 \cdot 10^{11}$ | nmol $d^{-1}$ |
| $F_{SGD}$ | SGD flux for entire bay | $9.7 \pm 8.3 \cdot 10^5$ | $2.7 \pm 11.8 \cdot 10^5$ | $3.5 \pm 0.8 \cdot 10^5$ | $m^3\ d^{-1}$ |

[1] Martin and Camacho, 2013
[2] USGS National Water System Information
[3] Fiket et al., 2017

Ultimately, the SGD water volume flux values for $^{224}$Ra and $^{223}$Ra were high, where $^{223}$Ra uncertainty was greater than the actual value determined. The large error here is mainly attributed to the sediment diffusion determination. In previous work using a similar incubation method to what was employed here, the authors gave the method a 50% uncertainty which was then adapted here (Rodellas et al., 2015). This uncertainty was chosen in the original work based on the error associated with scaling up small in-lab incubations to the entire bay floor and the uncertainty of how representative the sediments sampled would be for the entire bay. In St. Louis Bay, samples were chosen to represent various sediment compositions found in the bay based on an existing surficial sediment map for the bay. The samples taken to determine the radium and barium inventories in the bay were averaged and their uncertainty was one standard deviation for

the set of samples (n = 9). The uncertainty given here is the main reason that $^{223}$Ra has a higher uncertainty than $^{224}$Ra since the samples varied more. For barium, since the sediment diffusion was adapted from existing literature, the uncertainty used for radium was not adapted for this value. The literature used (Fiket et al., 2017) did not provide an uncertainty value. From these final values, there is still evidence for SGD. Although $^{223}$Ra had such a high uncertainty going well into the negative values, it was used to calculate SGD chemical fluxes for nutrients and methane. The caveat to those values derived using it is that their uncertainty would also be very high with the lower end being well into negative values. Considering the other two values, there does still seem to be a non-zero flux of SGD water volume flux. Even with the wide range of the $^{224}$Ra-derived value, with the lower being just 10% of the calculated flux, this value could still be significant for the chemical fluxes of interest from groundwater as will be discussed in later sections.

### 3.3.5 Spatial variation of SGD within SLB

While the mass balance approach used $^{224}$Ra, $^{223}$Ra, and Ba inventories for the entire bay, some work was done to determine if SGD flux occurs unevenly across the bottom of SLB. The radium surface water distributions from Section 3.1 show that radium activity does seem to be higher on the west side of the main portion of the bay. However, given the non-gridded station layout and low concentration of points, a conclusion based on this information is uncertain and difficult to verify. To better determine the spatial variability, a continuous radon survey was also done to look at relative highs and lows of $^{222}$Rn. This radioisotope is a gas that is a decay daughter of $^{226}$Ra and is a useful groundwater tracer given its short half-life ($t_{1/2}$ = 3.8 d), enrichment

in groundwater compared to surface water, and chemical inertness (Burnett and Dulaiova, 2003). Due to constraints with desiccant needed in the experiment and time, the survey was limited to a main transect north and south along the bay.

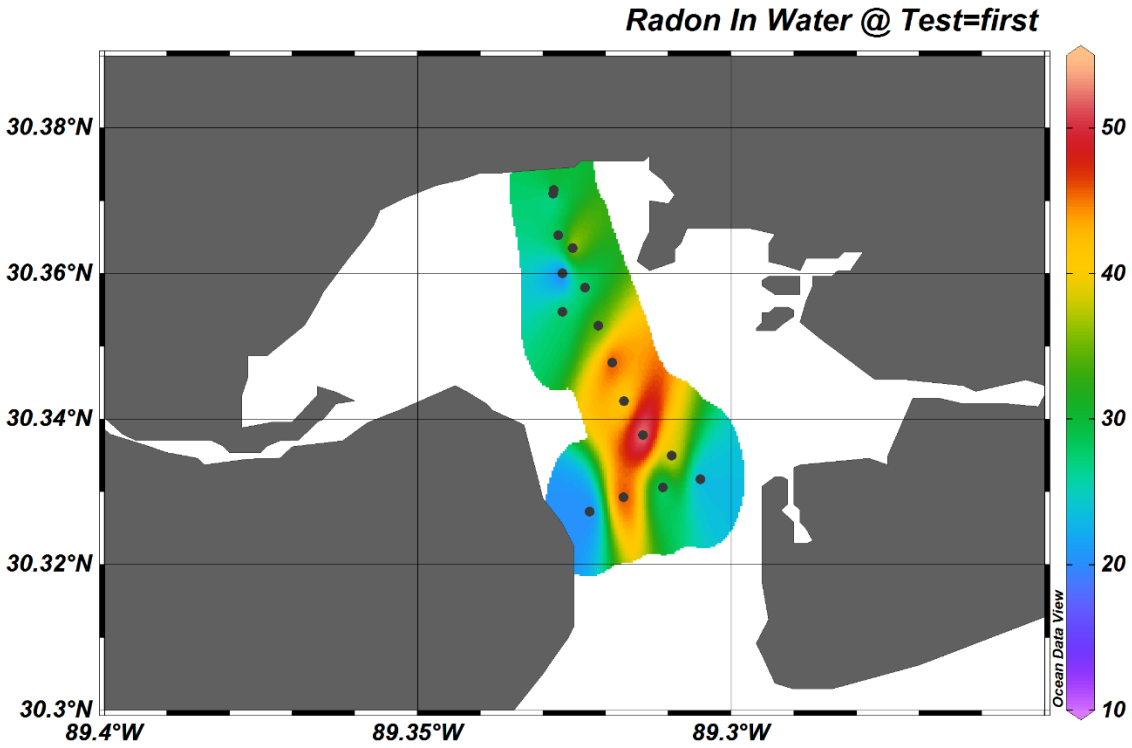


Figure 3.9 *Map of $^{222}Rn$ survey results in Bq $m^{-3}$*

From the radon survey (Figure 3.9), it seems that there is a hot spot of radon near the center of the bay. This hotspot was then also compared with a map of sediment distribution of the bay (Figure 3.10). Generally, SGD flux happens more readily in coarser grained sediments where the water can move more freely, although radium diffusion from sediments is much higher in muddy sediments. The sediment diffusion could affect the $^{222}Rn$ results because the parent isotope may be released more readily in areas with more fine-grained sediments. While this hotspot area seems to coincide with a

finer-grained region of the bay, this relationship is not supported along the north of the bay where sediments are also relatively fine but $^{222}Rn$ was low.

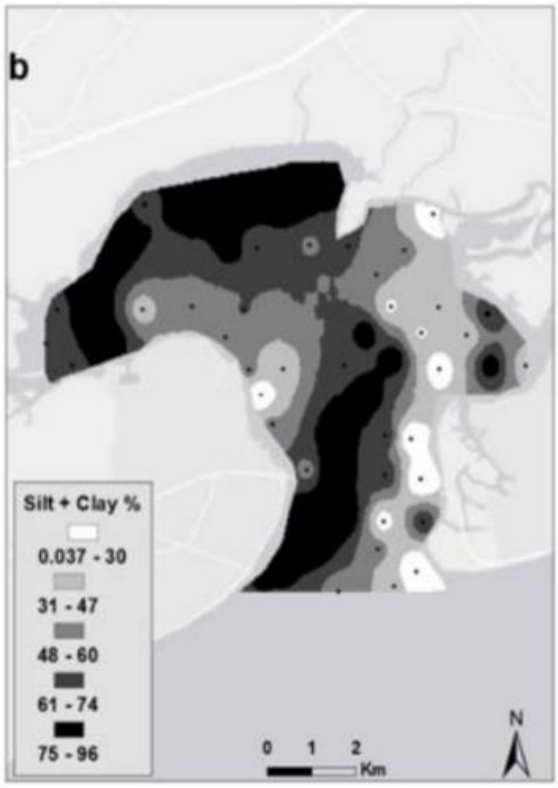


Figure 3.10 *Map of SLB subsurface sediment composition (Bera 2014)*

Another feature of SLB that was examined as evidence for SGD variability was paleochannels. Paleochannels are past riverbeds that have filled with sediment over time. In many areas, the sediment that fills these past riverbeds is different in composition to the channel walls and can create an area of subsurface preferential flow for SGD (Mulligan et al., 2007). In this case, the ones here are underneath the SLB and some have been identified from previous work (Dike et al., 2019). Figure 3.11 is a map of proposed paleochannels within St. Louis Bay from the MIS 1/MIS 2 sequence boundary. The different colors indicate the depth of the boundary between Marine Isotope Stages 1 and 2. This boundary is of interest because it is shallower and will have a larger effect on

groundwater flow at the bay surface than deeper sequence boundaries. The main channels identified do not seem to correlate strongly with the radon survey data. While the high point in the radon survey does seem to correlate with a topographic low in what looks like a paleochannel, the radon activity high does not continue along the length of that channel.

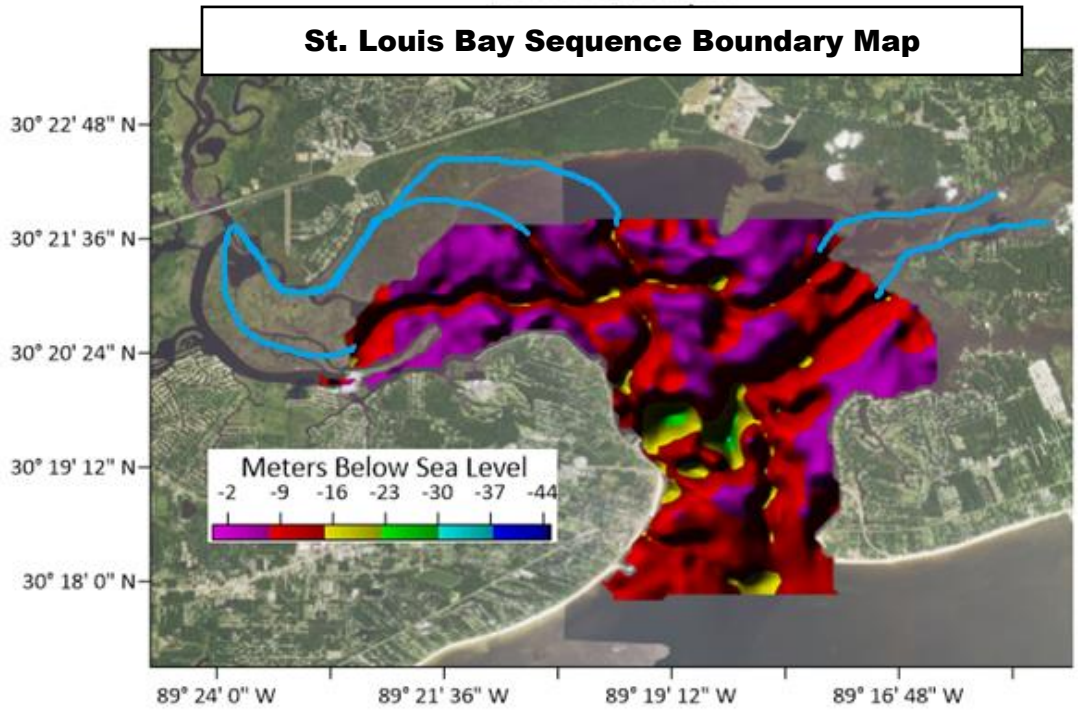


Figure 3.11 *Map of St. Louis Bay MIS 1/MIS 2 Sequence Boundary (Dike et al., 2019)*

Note: Map shows the sequence boundary between MIS 1 and MIS 2, showing subsurface paleochannels from this time period.

Another factor to consider in the spatial variability in the bay is the effect of dredging activity. Dredging of the coastal subsurface is thought to cause anthropogenically driven groundwater discharge (Burnett et al., 2006; Santos et al., 2008; Douglas et al., 2020). To explore this idea, the radon surface data was compared to the map shown in Figure 3.12 which shows the dredged channels in the bay with the double

dashed lines, extending to both the Wolf and Jourdan River openings as well as Bayou Portage.

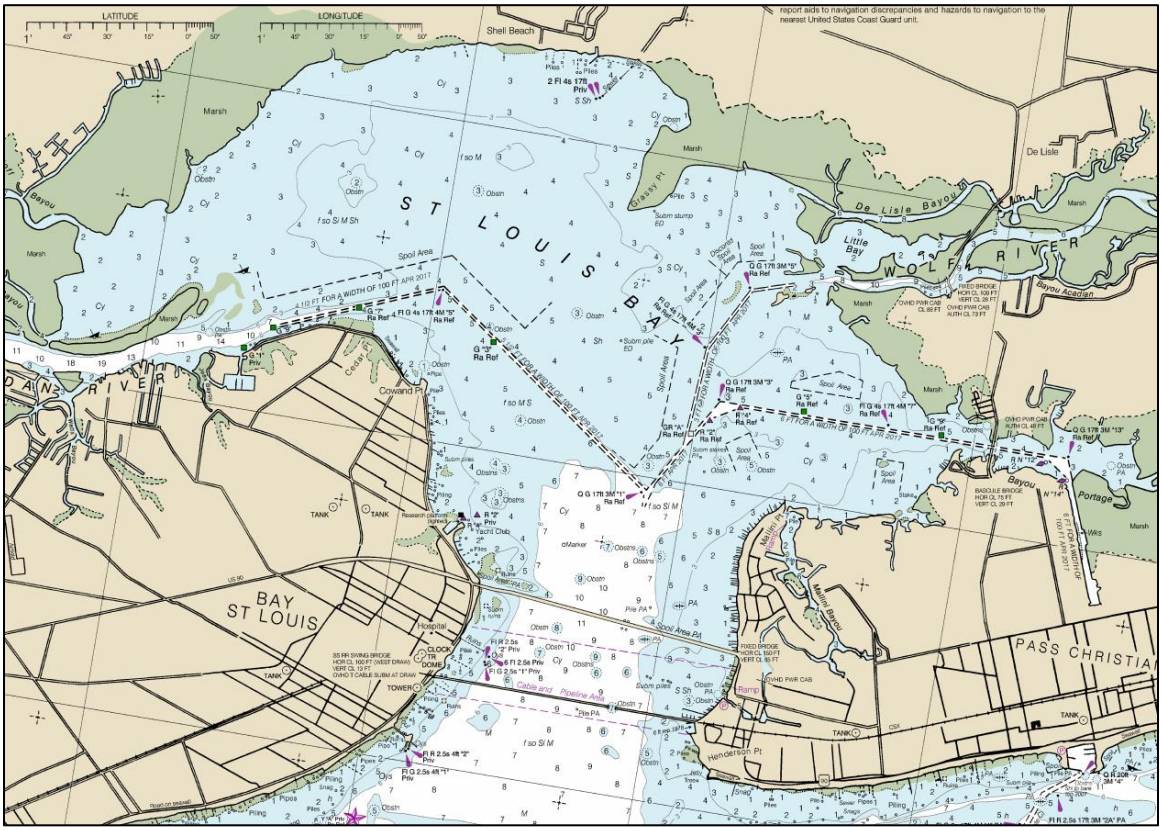


Figure 3.12 *Nautical map of St. Louis Bay*

The above nautical map shows St. Louis Bay with the dredging channels shown as black double dashed lines

Source: NOAA National Ocean Service Coast Survey

Overall, while no hard conclusions could be reached about the reasons for spatial variability in SGD rates across St. Louis Bay, the variation in sediment distribution and subsurface geology provides evidence that SGD is likely not uniform throughout the bay. However, it is important to note that the SGD flux calculations derived from the mass balance approach are an average for the entire bay and that flux rate is not likely the same over every area of the bay.

### 3.3.6 Comparing SGD flux to previous research

To ensure that the data derived from this study fell within reasonable amounts, it was compared to values found in other estuaries from previously published literature (Table 3.4). The literature to compare to this study was chosen based on the use of a similar mass balance approach using radium isotopes and that the data being compared among the study is available such as the water age. They were also chosen given that the estuary being studied was roughly the size of St. Louis Bay. SGD flux was normalized for the surface area of the respective study site to compare between studies.

Compared to the other studies chosen, SGD in the bay was relatively low but was not unusually higher or lower than the values found at other sites. One of the other terms compared was sediment diffusion rates for $^{224}Ra$. Since this term comprised a large proportion of the radium inventory in the bay and was extrapolated from a much smaller in-lab incubation experiment, it was important to compare the diffusion rate to other literature. In this case, the data from other literature varies over an order of magnitude. Based on the data from the Port of Mao (Rodellas et al., 2015) and Waquoit Bay (Charette et al., 2001), it was noted that diffusion is not typically a major radium source for an estuary though it is relatively more important for $^{224}Ra$ than longer lived radium isotopes. While Charette et al. (2001) measured $^{226}Ra$, Rodellas et al. (2015) measured $^{224}Ra$ and sediment diffusion was a much larger proportion of the $^{224}Ra$ inventory. It has also been found that sediment diffusion plays a much larger role in estuaries covered by fine grained sediments where diffusive flux from fine grained sediment can be 1-2 orders of magnitude higher than those from coarse grained sediment (Garcia-Orellana et al., 2014). It should also be noted that in the Port of Mao (Rodellas et al., 2015), the sediment

diffusion measurement was determined using an incubation where the overlying water used replaced at set intervals which increased the diffusive gradient and was presented as a maximum estimate of diffusion. The other sediment diffusion value being compared in Table 3.4 is from Alfacs Bay (Rodellas et al., 2017). In Alfacs Bay, the diffusion rate was determined using the molecular diffusivity of $^{224}$Ra at temperatures appropriate to the study site using the gradient of $^{224}$Ra concentration between the porewater and overlying bay waters and a ~10 cm diffusion scale. While the authors noted that this calculation would have high uncertainty, sediment diffusion was a small portion of the inventory (<3%) and the uncertainty would not greatly impact the overall radium inventory.

Table 3.4

*Data comparisons from other SGD studies*

| | St. Louis Bay | Alfacs Bay[a] | Port of Mao[b] | Waquoit Bay[c] | Units |
|---|---|---|---|---|---|
| Study Site Surface Area | $3.98 \cdot 10^7$ | $4.90 \cdot 10^7$ | $3.00 \cdot 10^6$ | $3.86 \cdot 10^6$ | $m^2$ |
| SGD Flux | 0.007-0.024 | 0.0006-0.0008 | 0.007* | 0.0096 | $m^3\ d^{-1}\ m^{-2}$ |
| $^{224}$Ra Sediment Diffusion | 170 | 1.2-2.7 | 110 | NA | dpm $m^{-2}\ d^{-1}$ |

[a] Rodellas et al., 2017
[b] Rodellas et al., 2015
[c] Charette et al., 2001
* This study measured multiple SGD fluxes at different times of the year. The July 2010 sampling period was chosen for comparison here.
NA: Not available

### 3.4 Biogeochemical Fluxes from Groundwater in St. Louis Bay

As mentioned before, a secondary step of this project is characterizing component fluxes associated with SGD. Looking at how nutrient flux correlates to the amount of SGD in a sample would provide information about how the groundwater nutrient compares to river flux. Once the SGD flux was calculated, biogeochemical fluxes could

then be calculated as well by using the SGD rate and the concentration of the substance of interest found in groundwater using the following equation:

$$F_C = F_{SGD} \times [C]$$

The biogeochemical fluxes ($F_C$) were calculated for the concentration [C] of the component fluxes of interest in the following sections.

### 3.4.1 Nutrient flux from SGD

Nutrient fluxes were calculated for nitrate, nitrite, ammonium, phosphate, and silicate, using the groundwater endmember concentrations. Table 3.5 summarizes the calculated fluxes from each mass balance. The numbers are presented in kmol $d^{-1}$. Also shown in Table 3.5 are nutrient fluxes calculated for total river input of the Wolf and Jourdan Rivers. Based on these data, SGD delivers more nitrate, phosphate, and silicate to the bay while the rivers deliver more ammonium and nitrite (Figure 3.13). Even when accounting for the uncertainty of the SGD water volume flux, the nutrient delivery is still significant because even at the lower range of uncertainty, excluding $^{223}Ra$, SGD is still inputting more $NO_3$, $PO_4$, and $SiO_3$ than the rivers.

The total inorganic N flux estimates from groundwater range from 430 to 1510 μmol $m^{-2}$ $d^{-1}$. Comparing this range to data from other studies summarized in Slomp and Cappellen (2004), the data falls in the middle of the range found in previous literature (see Table A.5 in the Appendix for a copy of the summary table found in the referenced literature). The same can be said for the total inorganic P flux which was about 15-50 μmol $m^{-2}$ $d^{-1}$. The N/P ratio of 29 for the groundwater indicates an oxic subterranean environment given that N is transported conservatively while P is largely removed (Slomp and Van Capellen, 2004). This conclusion makes sense given that the

groundwater was sampled from a relatively shallow environment along the edge of the bay.

Table 3.5

*Nutrient fluxes from SGD and total river input*

| | Groundwater Concentration | Nutrient Flux from SGD (as determined by each tracer) | | | River Concentration | Nutrient Flux from Rivers |
|---|---|---|---|---|---|---|
| | | $^{224}Ra$ | $^{223}Ra$ | Ba | | |
| | µM | kmol $d^{-1}$ | kmol $d^{-1}$ | kmol $d^{-1}$ | µM | kmol $d^{-1}$ |
| $NO_3$ | 62 | 60 ± 52 | 17 ± 73 | 22 ± 5 | 1.5 | 1.2 |
| $NO_2$ | 0.10 | 0.10 ± 0.08 | 0.03 ± 0.12 | 0.04 ± 0.008 | 0.23 | 0.18 |
| $NH_4$ | 0.11 | 0.11 ± 0.09 | 0.03 ± 0.13 | 0.04 ± 0.008 | 0.24 | 0.19 |
| $PO_4$ | 2.1 | 2.1 ± 1.7 | 0.6 ± 2.5 | 0.8 ± 0.2 | 0.04 | 0.03 |
| $SiO_3$ | 43 | 42 ± 36 | 12 ± 50 | 15 ± 3 | 2.55 | 2.03 |

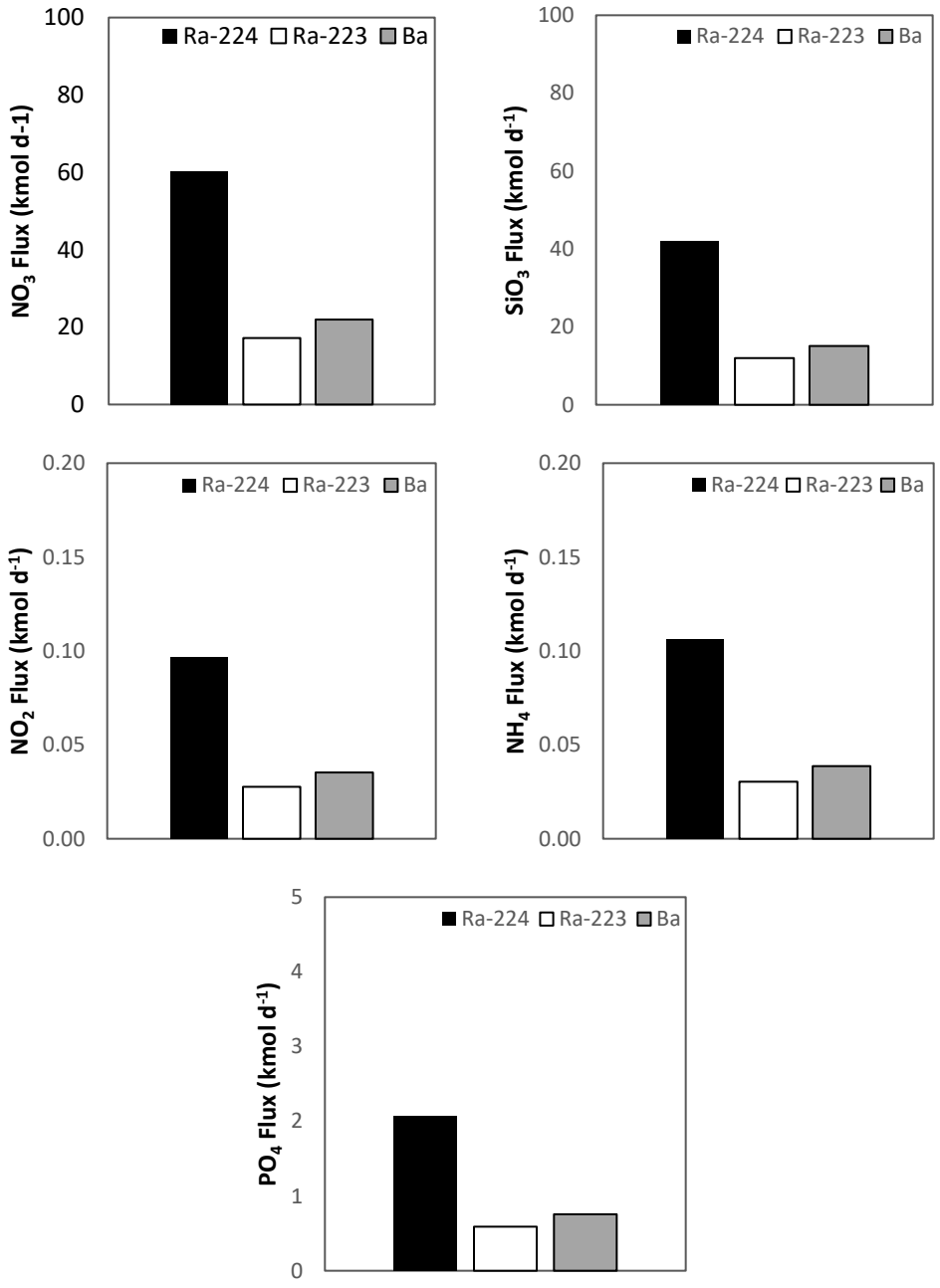


Figure 3.13 *Nutrient fluxes from each mass balance approach.*

### 3.4.2 Methane flux from SGD

Previous work has been done in St. Louis Bay regarding methane dynamics. The role of SGD and methanogenesis in sediments was speculated, but concrete conclusions were not found (Roberts, 2014). In the present study, where SGD rates have been

calculated, methane flux from can be estimated. To determine a groundwater methane endmember, other data (unpublished) from the Mississippi Gulf Coast region had to be used since the instrument used to analyze methane samples was not available at the time of the groundwater sampling. Without directly measuring the groundwater endmember within the bay itself, the values presented here are best estimates.

Using an endmember concentration of 2500 nM and the three mass balance approaches, methane flux would be 2411 mol $d^{-1}$ ($^{224}$Ra), 689 mol $d^{-1}$ ($^{223}$Ra), and 864 mol $d^{-1}$ (Ba) respectively for the entire bay with the average of the three values being 1300 mol $d^{-1}$. These values fall within the estimate given from previous research in the bay where total methane input from the bottom of the bay was estimated to be somewhere in the range of 120-16,000 mol $d^{-1}$ when accounting for temporal and spatial variability (Roberts, 2014). When accounting for the uncertainty of the SGD water volume flux, the methane fluxes based on the $^{224}$Ra and Ba mass balances still fall within this range.

# CHAPTER IV - CONCLUSIONS

From this study, there is evidence that submarine groundwater discharge plays an important role in St. Louis Bay. Using all three tracers, $^{224}Ra$, $^{223}Ra$, and Ba, there is a measurable amount of SGD with average water volume flux of $5.3 \cdot 10^5$ $m^3$ $d^{-1}$, which was about two-thirds of the river water flux. While it was hypothesized that the main radium input to the bay would be from SGD, it turned out to be diffusion from sediments that was the major source. The large diffusive fluxes are from the high proportion of fine-grained sediments along the bottom of the bay. I also hypothesized that barium would be primarily from SGD. From this study, it was found that rivers and SGD contributed similar amounts of barium to St. Louis Bay.

While the total amount of SGD for St. Louis Bay was estimated, results of spatial variability of SGD input in the bay were less conclusive. While the $^{222}Rn$ survey data suggested an SGD hotspot near the middle of the bay, a higher flux of SGD in the area is not supported by evidence from surficial sediment distribution or preliminary paleochannel mapping.

SGD delivers approximately 1300 mol $d^{-1}$ of methane to St. Louis Bay. The mass balance approach used in this study was able to narrow down the estimated input for the sampling period used in this study compared to the previous estimate of 120-16,000 mol $d^{-1}$ input from the bottom of the bay where the previous estimate reflects both temporal and spatial variability of sampling within the bay. Nutrient delivery by SGD was also significant especially for nitrate. Nitrate inputs into the bay were about 17-60 kmol $d^{-1}$. Based on the data collected for the Wolf River, nitrate flux from rivers was about 1.2 kmol $d^{-1}$. As hypothesized, SGD seems to be a major input for nitrate into the bay. SGD

was also a significant source of silicate and phosphate compared to rivers with 12-42 kmol $d^{-1}$ and 0.6-2.1 kmol $d^{-1}$ input respectively. For ammonium and nitrite, SGD was not found to be a significant source and was less than the input from rivers. Since nutrient loading is a concern in St. Louis Bay for eutrophication, understanding the role SGD plays is an important consideration for managing this environmental issue.

Given the conclusions found here, future work and research could be aimed at now characterizing other characteristics of the SGD entering SLB. Given that there are now SGD water volume flux estimates, measuring other chemical components of the groundwater endmember could then produce flux other estimates. For instance, knowing fecal coliform groundwater concentrations could be used to determine their flux from SGD. If it is found that SGD is a significant source of fecal coliform, it would suggest that leaky septic tanks around St. Louis Bay are a contributing factor to the fecal coliform water quality issues in the bay. This idea could be extended to any number of SGD chemical components of interest. The groundwater endmember value can now be used to estimate the flux into the bay from groundwater of the chemical of interest.

To further address water quality and nutrient inputs to the bay, nitrogen isotope analysis of the inorganic N nutrient inputs to the bay could be used to determine the source of the nutrients in the groundwater. Possible sources include percolation of nitrogen enriched water, possibly from fertilized farmland. Another source could be remineralization of organic matter in the groundwater. Nitrogen isotope data could help elucidate the source and provide more information regarding the human impact on St. Louis Bay.

# APPENDIX A – Supplemental Data

## Table A.1

*All data from the St. Louis Bay sampling*

| | | | | | | | | | Radium | | | Nutrients (µM) | | | | | |
|---|---|---|---|---|---|---|---|---|---|---|---|---|---|---|---|---|---|
| Site ID | Sampling Date | Lat | Lon | Time | S | T (°C) | Ba (nM) | CH4 (nM) | $^{224}$Ra (dpm/ 100L) | $^{223}$Ra (dpm/ 100L) | $^{224}$Ra/ $^{223}$Ra | $PO_4$ | $SiO_3$ | $NH_4$ | $NO_x$ | $NO_3$ | $NO_2$ |
| SLB-1 | 6/7/2017 | 30.31433 | -89.30508 | 9:01 | 2 | 25.0 | 177 | 19 | 27 | 2.7 | 10 | 0.44 | 28.36 | 1.69 | 1.77 | 1.57 | 0.20 |
| SLB-2 | 6/7/2017 | 30.35533 | -89.29169 | 10:15 | 0 | ** | 212 | 270 | 30 | 1.7 | 18 | 0.12 | 2.39 | 0.96 | 1.31 | 1.12 | 0.18 |
| SLB-3 | 6/7/2017 | 30.35731 | -89.32397 | 11:15 | 0 | ** | 138 | 11 | 21 | 0.9 | 23 | 0.15 | 21.96 | 0.74 | 0.68 | 0.50 | 0.18 |
| SLB-4 | 6/7/2017 | 30.34233 | -89.36833 | 12:37 | 0 | ** | 133 | ǂ | 28 | 2.6 | 11 | 0.39 | 0.97 | 0.39 | 4.28 | 4.00 | 0.28 |
| SLB-5 | 6/7/2017 | 30.33697 | -89.32331 | 13:02 | 0 | ** | 120 | 44 | 15 | 0.3 | 56 | 0.36 | 6.18 | 1.32 | 3.33 | 3.02 | 0.32 |
| SLB-3 | 7/31/2017 | 30.35787 | -89.32497 | 11:44 | 18 | 27.9 | 317 | 133 | 70 | 5.8 | 12 | 0.88 | 53.41 | 1.15 | 0.33 | 0.25 | 0.08 |
| SLB-5 | 7/31/2017 | 30.33661 | -89.32349 | 13:22 | 16 | 28.4 | 254 | 53 | 51 | 3.1 | 16 | 1.10 | 64.54 | 1.37 | 0.52 | 0.42 | 0.10 |
| SLB-6 | 7/31/2017 | 30.36892 | -89.35376 | 8:51 | 8.3 | 28.3 | 346 | 257 | 79 | 6.6 | 12 | 0.17 | 71.73 | 1.64 | 0.36 | 0.23 | 0.13 |
| SLB-7 | 7/31/2017 | 30.36850 | -89.35358 | 9:21 | 8.3 | 28.3 | 313 | 132 | 60 | 5.6 | 11 | 0.17 | 64.12 | 1.58 | 0.33 | 0.23 | 0.10 |
| SLB-8 | 7/31/2017 | 30.36772 | -89.35328 | 9:45 | 8.7 | 28.3 | 291 | 73 | 60 | 3.5 | 17 | 0.15 | 52.44 | 1.96 | 0.35 | 0.25 | 0.10 |
| SLB-9 | 7/31/2017 | 30.37479 | -89.33181 | 10:18 | 14 | 27.8 | 358 | 416 | 107 | 7.4 | 14 | 0.36 | 62.46 | 1.66 | 0.86 | 0.39 | 0.48 |
| SLB-10 | 7/31/2017 | 30.37439 | -89.33203 | 10:43 | 14 | 28.5 | 349 | 354 | 101 | 3.4 | 30 | 0.30 | 63.78 | 1.46 | 0.34 | 0.21 | 0.14 |
| SLB-11 | 7/31/2017 | 30.37331 | -89.33249 | 11:12 | 12 | 28.2 | 305 | 88 | 65 | 2.8 | 23 | 0.22 | 54.47 | 1.49 | 0.28 | 0.16 | 0.11 |
| SLB-12 | 7/31/2017 | 30.33956 | -89.33282 | 12:15 | 10 | 28.2 | 268 | 77 | 63 | 2.8 | 22 | 0.43 | 55.18 | 1.33 | 0.31 | 0.21 | 0.10 |
| SLB-13 | 7/31/2017 | 30.33951 | -89.33182 | 12:43 | 12 | 28.4 | 241 | 48 | 49 | 1.9 | 25 | 0.51 | 56.64 | 1.32 | 0.34 | 0.24 | 0.10 |

Table A.1 (continued).

| | | | | | | | | | Radium | | | | Nutrients (μM) | | | | |
|---|---|---|---|---|---|---|---|---|---|---|---|---|---|---|---|---|---|
| Site ID | Sampling Date | Lat | Lon | Time | S | T (°C) | Ba (nM) | CH4 (nM) | $^{224}$Ra (dpm/ 100L) | $^{223}$Ra (dpm/ 100L) | $^{224}$Ra/ $^{223}$Ra | $PO_4$ | $SiO_3$ | $NH_4$ | $NO_x$ | $NO_3$ | $NO_2$ |
| SLB-5 | 9/20/2017 | 30.33659 | -89.32337 | 13:17 | 3 | 29.5 | 283 | 26 | 43 | 2.9 | 15 | 0.31 | 61.17 | 1.49 | 0.33 | 0.20 | 0.13 |
| SLB-6 | 9/20/2017 | 30.36874 | -89.35378 | 9:02 | 2 | 28.6 | 306 | 158 | 51 | 2.5 | 20 | 0.15 | 32.94 | 1.42 | 0.44 | 0.29 | 0.15 |
| SLB-7 | 9/20/2017 | 30.36850 | -89.35349 | 9:37 | 3 | 29.1 | 307 | 72 | 62 | 2.5 | 24 | 0.16 | 40.59 | 1.40 | 0.46 | 0.35 | 0.12 |
| SLB-8 | 9/20/2017 | 30.36776 | -89.35329 | 10:09 | 3 | 29.7 | 309 | 74 | 62 | 2.6 | 24 | 0.17 | 45.74 | 1.31 | 0.43 | 0.32 | 0.11 |
| SLB-9 | 9/20/2017 | 30.37482 | -89.33174 | 10:43 | 4 | 29.0 | 336 | 70 | 120 | 9.2 | 13 | 0.14 | 35.52 | 3.70 | 0.75 | 0.60 | 0.15 |
| SLB-10 | 9/20/2017 | 30.37450 | -89.33202 | 11:11 | 3 | 29.1 | 328 | 82 | 121 | 7.1 | 17 | 0.16 | 61.44 | 3.94 | 0.69 | 0.55 | 0.14 |
| SLB-11 | 9/20/2017 | 30.37336 | -89.33257 | 11:40 | 3 | 29.8 | 323 | 66 | 67 | 4.8 | 14 | 0.19 | 48.37 | 1.41 | 0.33 | 0.21 | 0.12 |
| SLB-12 | 9/20/2017 | 30.33948 | -89.33280 | 12:15 | 4 | 29.3 | 284 | 61 | 38 | 4.5 | 8 | 0.25 | 67.21 | 1.45 | 0.31 | 0.18 | 0.14 |
| SLB-13 | 9/20/2017 | 30.33959 | -89.33173 | 12:46 | 4 | 29.1 | 285 | 47 | 56 | 3.1 | 18 | 0.28 | 76.91 | 1.41 | 0.39 | 0.25 | 0.14 |
| SLB-1 | 4/23/2018 | 30.31410 | -89.30459 | 14:08 | 8.6 | 21.4 | * | 19 | 38 | 2.1 | 18 | 0.45 | 53.55 | 0.10 | 1.61 | 1.51 | 0.10 |
| SLB-2 | 4/23/2018 | 30.35608 | -89.29119 | 12:42 | 2.4 | 21.5 | * | 39 | 37 | 0.8 | 44 | 0.19 | 53.77 | 0.08 | 0.32 | 0.24 | 0.09 |
| SLB-3 | 4/23/2018 | 30.35810 | -89.32362 | 11:22 | 2.1 | 20.2 | * | 39 | 28 | 1.2 | 23 | 0.29 | 29.95 | 0.22 | 3.15 | 2.93 | 0.23 |
| SLB-4 | 4/23/2018 | 30.34060 | -88.63903 | 9:11 | 0.2 | 19.3 | * | 92 | 15 | 0.2 | 64 | 0.26 | 7.73 | 0.36 | 2.70 | 2.33 | 0.37 |
| SLB-5 | 4/23/2018 | 30.33699 | -89.32325 | 13:32 | 6.2 | 21.9 | * | 35 | 38 | 1.1 | 34 | 0.25 | 51.72 | 0.16 | 2.27 | 2.11 | 0.17 |
| SLB-14 | 4/23/2018 | 30.35070 | -89.34828 | 9:45 | 0.3 | 19.5 | * | 61 | 13 | 0.6 | 21 | 0.31 | 9.11 | 0.31 | 3.13 | 2.81 | 0.32 |
| SLB-15 | 4/23/2018 | 30.36314 | -89.32468 | 10:15 | 1.9 | 20.5 | * | 31 | 35 | 0.6 | 62 | 0.22 | 39.71 | 0.24 | 2.48 | 2.23 | 0.25 |
| SLB-16 | 4/23/2018 | 30.36283 | -89.34618 | 10:46 | 1.5 | 20.8 | * | 46 | 25 | 0.8 | 30 | 0.15 | 42.08 | 0.23 | 1.55 | 1.33 | 0.22 |

Table A.1 (continued).

| | | | | | | | | | Radium | | | Nutrients (µM) | | | | | |
|---|---|---|---|---|---|---|---|---|---|---|---|---|---|---|---|---|---|
| Site ID | Sampling Date | Lat | Lon | Time | S | T (°C) | Ba (nM) | CH4 (nM) | $^{224}$Ra (dpm/ 100L) | $^{223}$Ra (dpm/ 100L) | $^{224}$Ra/ $^{223}$Ra | $PO_4$ | $SiO_3$ | $NH_4$ | $NO_x$ | $NO_3$ | $NO_2$ |
| SLB-17 | 4/23/2018 | 30.33201 | -89.29568 | 13:06 | 4.8 | 21.3 | * | 34 | 30 | 0.7 | 45 | 0.21 | 51.36 | 0.05 | 4.32 | 4.26 | 0.06 |
| SLB-18 | 4/23/2018 | 30.30593 | -89.30928 | 14:36 | 8.4 | 21.7 | * | 31 | 37 | 0.5 | 68 | 0.24 | 48.32 | 0.04 | 0.44 | 0.39 | 0.05 |
| WR | 4/23/2018 | 30.36451 | -89.26678 | 12:04 | 0.2 | 21.0 | * | 546 | 20 | 0.5 | 38 | 0.09 | 34.97 | 0.07 | 1.81 | 1.72 | 0.09 |
| SLB-1 | 8/10/2018 | 30.31406 | -89.30448 | 9:37 | 21 | 30.7 | 471 | 83 | 85 | 4.6 | 18 | 1.14 | 33.02 | 0.04 | 0.40 | 0.34 | 0.06 |
| SLB-2 | 8/10/2018 | 30.35623 | -89.29099 | 11:27 | 19 | 30.2 | 506 | 60 | 100 | 5.7 | 18 | 1.07 | 34.94 | 0.02 | 0.53 | 0.49 | 0.04 |
| SLB-3 | 8/10/2018 | 30.35816 | -89.32433 | 11:45 | 19 | 30.7 | 498 | 26 | 93 | 4.6 | 20 | 1.17 | 34.90 | 0.05 | 0.39 | 0.33 | 0.06 |
| SLB-4 | 8/10/2018 | 30.34057 | -89.36111 | 8:57 | 16 | 29.8 | 515 | 64 | 94 | 5.2 | 18 | 0.90 | 35.80 | 0.07 | 0.36 | 0.28 | 0.08 |
| SLB-5 | 8/10/2018 | 30.33693 | -89.32292 | 9:21 | 21 | 30.1 | 483 | 114 | 116 | 7.6 | 15 | 1.41 | 30.28 | 0.02 | 0.52 | 0.50 | 0.03 |
| SLB-14 | 8/10/2018 | 30.35069 | -89.34843 | 12:33 | 17 | 31.1 | 514 | 40 | 92 | 4.0 | 23 | 0.97 | 34.17 | 0.02 | 0.42 | 0.39 | 0.03 |
| SLB-15 | 8/10/2018 | 30.36772 | -89.32372 | 12:00 | 18 | 30.7 | 517 | 27 | 95 | 4.8 | 20 | 0.39 | 17.82 | 0.04 | 0.18 | 0.13 | 0.06 |
| SLB-16 | 8/10/2018 | 30.36281 | -89.34663 | 12:15 | 18 | 31.2 | 515 | 35 | 86 | 5.0 | 17 | 1.02 | 34.66 | 0.01 | 0.31 | 0.28 | 0.03 |
| SLB-17 | 8/10/2018 | 30.33206 | -89.29561 | 11:08 | 20 | 30.4 | 478 | 22 | 74 | 3.2 | 23 | 1.21 | 32.76 | 0.04 | 0.42 | 0.37 | 0.05 |
| Rn-1 | 8/24/2018 | 30.32331 | -89.29420 | 11:20 | 19 | 29.9 | * | 46 | 44 | 1.9 | 24 | * | * | * | * | * | * |
| Rn-3 | 8/24/2018 | 30.37147 | -89.32824 | 12:52 | 16 | 29.9 | * | 31 | 239 | 6.9 | 34 | * | * | * | * | * | * |
| Rn-4 | 8/24/2018 | 30.94347 | -89.28892 | 11:45 | 17 | 29.3 | * | 25 | 223 | 10.0 | 22 | * | * | * | * | * | * |
| GW-1 | 8/29/2018 | 30.32441 | -89.32614 | 12:04 | 4.5 | 29.8 | 641 | * | 441 | 10.6 | 42 | 2.1 | 43.5 | 0.1 | 62.3 | 62.2 | 0.1 |
| WR-Diss | 11/11/2018 | 30.37791 | -89.23146 | 8:30 | 0 | 15.4 | 258 | * | 13 | 1.5 | 8 | 0.04 | 2.55 | 0.24 | 1.74 | 1.51 | 0.23 |

Table A.1 (continued).

| Site ID | Sampling Date | Lat | Lon | Time | S | T (°C) | Ba (nM) | CH4 (nM) | Radium | | | Nutrients (µM) | | | | | |
|---|---|---|---|---|---|---|---|---|---|---|---|---|---|---|---|---|---|
| | | | | | | | | | $^{224}$Ra (dpm/ 100L) | $^{223}$Ra (dpm/ 100L) | $^{224}$Ra/ $^{223}$Ra | $PO_4$ | $SiO_3$ | $NH_4$ | $NO_x$ | $NO_3$ | $NO_2$ |
| WR-Deso | 11/11/2018 | 30.37791 | -89.23146 | 8:30 | 0 | 15.4 | 323 | * | 21 | 0.2 | 136 | * | * | * | * | * | * |

* Not sampled
** Temperature sensor malfunction
ǂ Sample lost

Table A.2

*Summary table from Slomp and Van Cappellen (2004)*

| N-flux ($\mu$mol m$^{-2}$ d$^{-1}$) | P-flux ($\mu$mol m$^{-2}$ d$^{-1}$) | gw N/P (mol/mol) | Location | Geology | Redox conditions | Main N and P source | Reference |
|---|---|---|---|---|---|---|---|
| 24,000–72,000 | n.a. | >16 | Nauset Marsh Estuary, MA | Sandy sediment | gw oxic, sed n.a. | Sewage | Portnoy et al. (1998) |
| 550 | n.a. | n.a. | Waquoit Bay, MA | Fine to coarse sand and gravel | gw anoxic, sed oxic | Sewage | Charette et al. (2001) |
| 2200 | n.a. | n.a. | Town Cove, MA | Unconsolidated glacial sediment | n.a. | Sewage | Giblin and Gaines (1990) |
| 430–19,000 | n.a. | n.a. | Subestuaries, MA | Fine to coarse sand and gravel | n.a. | Sewage | Charette et al. (2001) and Valiela et al. (1992) |
| n.a. | n.a. | 270–5300 | Buttermilk Bay, MA | Medium to coarse sand | n.a. | Sewage | Weiskel and Howes (1992) |
| 301 | 0.58 | 519 | Bay side of Florida Keys | Carbonate aquifer | gw anoxic, sed anoxic | Sewage | Corbett et al. (1999) |
| Up to 53,000 | up to 410 | n.a. | Southern Chesapeake Bay | Alluvium | n.a. | Fertilizer | Gallagher et al. (1996) |
| n.a. | n.a. | ~100 | Discovery Bay, Jamaica | Limestone | | Human | Lapointe (1997) |
| n.a. | n.a. | 36 | Tomales Bay, California | Granite, sandstone, shale, alluvium | n.a. | Manure + sewage | Oberdorfer et al. (1990) |
| 1340 | 12 | 112 | Tumon Bay, Guam | Carbonate karst aquifer | n.a. | Natural | Matson (1993) |
| 920 | 37 | 25 | Inner Kahana Bay, Hawaii | Alluvium | n.a. | Natural | Garrison et al. (2003) |
| 160 | 9 | 18 | Middle Kahana Bay, Hawaii | Alluvium | n.a. | Natural | Garrison et al. (2003) |
| n.a. | n.a. | 5 | Sites near FSUML, Florida | Limestone and dolomite | gw anoxic | Natural | Bugna et al. (1996) |
| 2400 | 900 | 3 | North Inlet, South Carolina | Sand, gravel and clay | gw anoxic, sed anoxic | Natural | Krest et al. (2000) |
| n.a. | n.a. | 18 | Crescent Beach Florida | Limestone and dolomite | gw anoxic | Natural | Swarzenski et al. (2001) |
| n.a. | n.a. | 18 | Hasaki Beach, Japan | Sand | gw oxic + anoxic | n.a. | Uchiyama et al. (2000) |

# REFERENCES


Aminot A., Kirkwood D. S. and Kérouel R. (1997) Determination of ammonia in seawater by the indophenol-blue method: Evaluation of the ICES NUTS I/C 5 questionnaire. *Marine Chemistry* **56,** 59-75.

Bejannin S., van Beek P., Stieglitz T., Souhaut M. and Tamborski J. (2017) Combining airborne thermal infrared images and radium isotopes to study submarine groundwater discharge along the French Mediterranean coastline. *Journal of Hydrology: Regional Studies* **13,** 72-90.

Bera, G. (2014) The Delivery, Speciation, and Fate of Trace Elements in St. Louis Bay, Mississippi. Ph. D. thesis, Univ. of Southern Mississippi

Bera G., Yeager K. M. and Shiller A. M. (2018) Whether hurricane Katrina impacted trace metal and dioxin depositional histories in marshes of St. Louis Bay, Mississippi. *Science of The Total Environment* **624,** 517-529.

Bowman, J. (2010) Thousands of spotted seatrout released in St. Louis Bay. WLOX. http://www.wlox.com/story/13129952/thousands-of-spotted-seatrout-released-in-st-louis-bay

Burnett W. C., Bokuniewicz H., Huettel M., Moore W. S. and Taniguchi M. (2003) Groundwater and Pore Water Inputs to the Coastal Zone. *Biogeochemistry* **66,** 3-33.

Burnett W. C. and Dulaiova H. (2003) Estimating the dynamics of groundwater input into the coastal zone via continuous radon-222 measurements. *Journal of Environmental Radioactivity* **69**, 21-35.

Burnett W. C., Aggarwal P. K., Aureli A., Bokuniewicz H., Cable J. E., Charette M. A., Kontar E., Krupa S., Kulkarni K. M., Loveless A., Moore W. S., Oberdorfer J. A., Oliveira J., Ozyurt N., Povinec P., Privitera A. M. G., Rajar R., Ramessur R. T., Scholten J., Stieglitz T., Taniguchi M. and Turner J. V. (2006) Quantifying submarine groundwater discharge in the coastal zone via multiple methods. *The Science of the total environment* **367,** 498-543.

Charette M., Buesseler K. and Andrews J. (2001) Utility of Radium Isotopes for Evaluating the Input and Transport of Groundwater-Derived Nitrogen to a Cape Cod Estuary. *Limnology and Oceanography* **46,** 465-470.

Colbert D. and McManus J. (2005) Importance of seasonal variability and coastal processes on estuarine manganese and barium cycling in a Pacific Northwest estuary. *Continental shelf research* **25,** 1395-1414.

Dike, C., Wallace, D.J., Gal, N.S., Hollis, R.J., Anderson, J.B., and Minzoni, R.T. (2019) The evolution of St. Louis Bay, Mississippi since the MIS 2 Lowstand. *Coastal and Estuarine Research Federation Biennial Conference, Coastal sediment transport processes.* Mobile. (abstr.).

Douglas A. R., Murgulet D. and Peterson R. N. (2020) Submarine groundwater discharge in an anthropogenically disturbed, semi-arid estuary. *Journal of hydrology (Amsterdam)* **580,** 124369.

Dulaiova H., Camilli R., Henderson P. B. and Charette M. A. (2010) Coupled radon, methane and nitrate sensors for large-scale assessment of groundwater discharge and non-point source pollution to coastal waters. *Journal of Environmental Radioactivity* **101,** 553-563.

Fiket Ž, Fiket T., Ivanić M., Mikac N. and Kniewald G. (2019) Pore water geochemistry and diagenesis of estuary sediments—an example of the Zrmanja River estuary (Adriatic coast, Croatia). *J Soils Sediments* **19,** 2048-2060.

Garcia-Orellana J., Cochran J. K., Bokuniewicz H., Daniel J. W. R., Rodellas V. and Heilbrun C. (2014) Evaluation of 224Ra as a tracer for submarine groundwater discharge in Long Island Sound (NY). *Geochimica et Cosmochimica Acta* **141,** 314-330.

Garcia-Solsona E., Garcia-Orellana J., Masqué P. and Dulaiova H. (2008) Uncertainties associated with 223Ra and 224Ra measurements in water via a Delayed Coincidence Counter (RaDeCC). *Marine Chemistry* **109,** 198-219.

Gonneea M. E., Morris P. J., Dulaiova H. and Charette M. A. (2008) New perspectives on radium behavior within a subterranean estuary. *Marine Chemistry* **109,** 250-267.

Gonneea M., Mulligan A. and Charette M. (2013) Seasonal cycles in radium and barium within a subterranean estuary: Implications for groundwater derived chemical fluxes to surface waters. *Geochimica et Cosmochimica Acta* **119,** 164-177.

Grasshoff K., Ehrhardt M., Kremling K. (1983) *Methods of Seawater Analysis,* second revised and extended edition.

Joung D. and Shiller A. M. (2014) Dissolved barium behavior in Louisiana Shelf waters affected by the Mississippi/Atchafalaya River mixing zone. *Geochimica et Cosmochimica Acta* **141,** 303-313.

Knee K., Crook E., Hench J., Leichter J. and Paytan A. (2016) Assessment of Submarine Groundwater Discharge (SGD) as a Source of Dissolved Radium and Nutrients to Moorea (French Polynesia) Coastal Waters. *Estuaries and Coasts* **39,** 1651-1668.

Krest J. M., Moore W. S. and Rama (1999) 226Ra and 228Ra in the mixing zones of the Mississippi and Atchafalaya Rivers: indicators of groundwater input. *Marine Chemistry* **64,** 129-152.

Liefer J. D., MacIntyre H. L., Novoveská L., Smith W. L. and Dorsey C. P. (2009) Temporal and spatial variability in Pseudo-nitzschia spp. in Alabama coastal waters: A "hot spot" linked to submarine groundwater discharge? *Harmful Algae* **8,** 706-714.

Liu Z., Hashim N. B., Kingery W. L. and Huddleston D. H. (2010) Fecal coliform modeling under two flow scenarios in St. Louis Bay of Mississippi. *Journal of Environmental Science and Health, Part A* **45,** 282-291.

Martin J. L. and Camacho R. A. (2013) Hydrodynamic Modeling of First-Order Transport Timescales in the St. Louis Bay Estuary, Mississippi. *Journal of Environmental Engineering* **139,** 317-331.

Charette M., Buesseler K. and Andrews J. (2001) Utility of Radium Isotopes for Evaluating the Input and Transport of Groundwater-Derived Nitrogen to a Cape Cod Estuary. *Limnology and Oceanography* **46,** 465-470.

Monteil, D., Coburn N., Forkner, A. and Dimova, N. (2016) Examining the Importance of Submarine Groundwater Discharge (SGD) in a River Dominated Estuary: Example of Mobile Bay, AL. *2016 Ocean Sciences Meeting*. New Orleans. (abstr.)

Moore W. S. (1996) Large groundwater inputs to coastal waters revealed by 226Ra enrichments. *Nature* **380,** 612-614.

Moore W. S. and Arnold R. (1996) Measurement of 223Ra and 224Ra in coastal waters using a delayed coincidence counter. *Journal of Geophysical Research: Oceans* **101,** 1321-1329.

Moore W. S. (1999) The subterranean estuary: a reaction zone of ground water and sea water. *Marine Chemistry* **65,** 111-125.

Moore W. S., Blanton J. O. and Joye S. B. (2006) Estimates of flushing times, submarine groundwater discharge, and nutrient fluxes to Okatee Estuary, South Carolina. *Journal of Geophysical Research - Oceans* **111,** C09006.

Mulligan A. E., Evans R. L. and Lizarralde D. (2007) The role of paleochannels in groundwater/seawater exchange. *Journal of Hydrology* **335,** 313-329.

Null K., Dimova N., Knee K., Esser B., Swarzenski P., Singleton M., Stacey M. and Paytan A. (2012) Submarine Groundwater Discharge-Derived Nutrient Loads to San Francisco Bay: Implications to Future Ecosystem Changes. *Estuaries and Coasts* **35,** 1299-1315.

Roberts, H. (2014) Methane Dynamics in St. Louis Bay, Mississippi. Ph. D. thesis, Univ. of Southern Mississippi

Roberts H. M. and Shiller A. M. (2015) Determination of dissolved methane in natural waters using headspace analysis with cavity ring-down spectroscopy. *Analytica chimica acta* **856,** 68.

Russoniello C. J., Fernandez C., Bratton J. F., Banaszak J. F., Krantz D. E., Andres A. S., Konikow L. F. and Michael H. A. (2013) Geologic effects on groundwater salinity and discharge into an estuary. *Journal of Hydrology* **498,** 1-12.

Sadat-Noori M., Maher D. and Santos I. (2016) Groundwater Discharge as a Source of Dissolved Carbon and Greenhouse Gases in a Subtropical Estuary. *Estuaries and Coasts* **39,** 639-656.

Samadder R. K., Kumar S. and Gupta R. P. (2011) Paleochannels and their potential for artificial groundwater recharge in the western Ganga plains. *Journal of Hydrology* **400,** 154-164.

Sanial V., Shiller A. M. & Moore W. S. (2018) Hypoxia in the Mississippi Bight: Understanding the role of submarine groundwater discharge in a complex coastal ecosystem. *Goldschmidt*. Boston. (abstr.)

Santos I. R., Niencheski F., Burnett W., Peterson R., Chanton J., Andrade C. F. F., Milani I. B., Schmidt A. and Knoeller K. (2008) Tracing anthropogenically driven groundwater discharge into a coastal lagoon from southern Brazil. *Journal of hydrology (Amsterdam)* **353,** 275-293.

Schwartz M. C. (2003) Significant groundwater input to a coastal plain estuary: assessment from excess radon. *Estuarine, Coastal and Shelf Science* **56,** 31-42.

Shaw T. J., Moore W. S., Kloepfer J. and Sochaski M. A. (1998) The flux of barium to the coastal waters of the southeastern USA: the importance of submarine groundwater discharge. *Geochimica et Cosmochimica Acta* **62,** 3047-3054.

Shiller A. M. (1997) Dissolved trace elements in the Mississippi River: Seasonal, interannual, and decadal variability. *Geochimica et cosmochimica acta* **61,** 4321-4330.

Slomp C. P. and Van Cappellen P. (2004) Nutrient inputs to the coastal ocean through submarine groundwater discharge: controls and potential impact. *Journal of Hydrology* **295,** 64-86.

Veeramony J. and Blain C. A. The Role of River Discharge and Vertical Mixing Formulation on Barotropic Circulation in Bay St. Louis, MS. In *Estuarine and Coastal Modeling (2001)* (Anonymous). pp. 743-764.

Wiesenburg D. A. and Guinasso N. L. (1979) Equilibrium solubilities of methane, carbon monoxide, and hydrogen in water and sea water. *Journal of Chemical & Engineering Data* **24,** 356-360.